Purcell's swimmers in pairs

Purcell's swimmers in pairs

Rossella Attanasi [*]
Dipartimento di Matematica e Fisica "Ennio de Giorgi", Università del Salento, 73100 Lecce, Italy

Marta Zoppello [†]
Dipartimento di Scienze Matematiche "Giuseppe Luigi Lagrange", Politecnico di Torino, 10129 Torino, Italy

Gaetano Napoli [‡]
Dipartimento di Matematica e Applicazioni "Renato Caccioppoli", Università degli Studi di Napoli "Federico II", 80125 Napoli, Italy

(Received 3 September 2023; revised 13 December 2023; accepted 2 January 2024; published 6 February 2024)

We investigate the effects of hydrodynamic interactions between microorganisms swimming at low Reynolds numbers, treating them as a control system. We employ Lie brackets analysis to examine the motion of two neighboring three-link swimmers interacting through the ambient fluid in which they propel themselves. Our analysis reveals that the hydrodynamic interaction has a dual consequence: on one hand, it diminishes the system's efficiency; on the other hand, it dictates that the two microswimmers must synchronize their motions to attain peak performance. Our findings are further corroborated by numerical simulations of the governing equations of motion.

DOI: 10.1103/PhysRevE.109.024601

I. INTRODUCTION

Over the past two decades, the study of the swimming strategy of microorganisms has stimulated a wealth of scientific research on their optimal control and controllability [1,2]. One of the most remarkable phenomena exhibited by swimming microorganisms is the coordination of their beating cilia. Studying the interplay between coordination and hydrodynamic interactions among swimmers holds significant interest, as exemplified in Refs. [3–5]. Coordinated beating manifests in a diverse range of geometries and organisms. It can occur among hundreds of cilia on a single organism, as observed in Ref. [6], or even extend to flagella on distinct cells, such as in the case of mammalian spermatozoa swimming in close proximity [7]. Moreover, in Ref. [7] the large-scale coordination of sperm cells is shown to be governed solely by hydrodynamic interaction forces, rather than chemical signals. Moreover, theoretical studies underscore the role of hydrodynamic forces and fluctuations in optimizing the navigation of microswimmers [8,9].

Nowadays, with the latest advances in manufacturing, technology, and three-dimensional (3D) printing, robotic swimming has emerged as a dynamic field that can translate abstract mathematical models into tangible applications [10–13]. As a result, recent research has shown growing interest in exploring the intricate relationship between swimming and control theory in viscous fluid environments [14–16].

Driven by the potential for robotic applications [17–19], fabrication through chemical synthesis [20,21], and the well-documented phenomena of coordination among neighboring beating flagella [22], this work explores the interactions between two flagellar microswimmers swimming in close proximity. For instance, limited research has been conducted on the displacement of these systems under the influence of nonlocal hydrodynamic interactions. Hydrodynamic interactions often play a pivotal role in the development of mathematical models for these systems. For example, a recent study [23] examined two individually uncontrollable scallops swimming in close proximity and demonstrated that their hydrodynamic interaction enables controllability. Furthermore, the combination of hydrodynamic interaction and phase-shifted flagellar beats among the microswimmers provides the asymmetry necessary to violate Purcell's "Scallop Theorem" [24].

In this work, we examine the behavior of two nearly aligned Purcell three-link swimmers in mutual hydrodynamic interaction [25], within the low Reynolds number regime. To facilitate analytical progress, we adopt a minimal interaction model where only adjacent links between the swimmers engage in reciprocal interactions. Our approach uses tools from geometric control theory, enabling us to investigate comprehensive displacement patterns and identify the most efficient periodic control sequences.

The paper is organized as follows. In Sec. II we derive the governing equations of motion, which are subsequently reformulated as a linear control problem. In Sec. III, using Lie bracket analysis, we obtain analytical results for the displacement of the two swimmers, assuming periodic control gaits. Our findings reveal that maximum displacement is attained when the swimmers operate in phase-locked synchronization. This result aligns with the phase-locking phenomena observed in cilia or sperm cells swimming in close proximity [25,26]. In Sec. IV, we compare theoretical findings with

[*]rossella.attanasi@unisalento.it
[†]marta.zoppello@polito.it
[‡]gaetano.napoli@unina.it

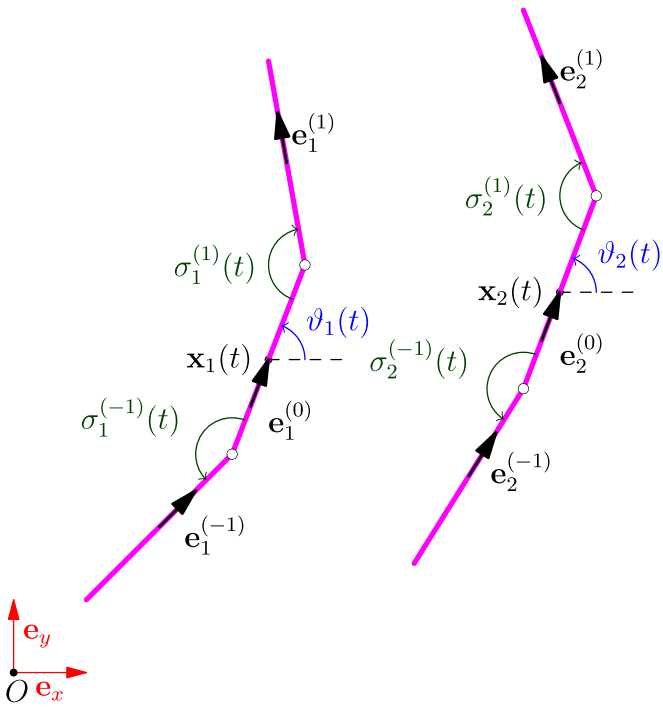

FIG. 1. Schematic representation of two three-links microswimmers.

numerical simulations of the motion equations. In conclusion, the four Appendixes elaborate on the technical aspects of the calculations.

II. MATHEMATICAL SETTING

In this section, we formulate the equations of motion for a pair of Purcell's swimmers, namely two three-link microswimmers immersed in a viscous fluid, swimming at a sufficiently close distance and nearly aligned.

One of the most challenging aspects of applying control theory to accurately solve motion planning or optimal control problems is the complexity of the hydrodynamic forces exerted by the fluid on the swimmer as its shape changes. Resistive force theory [27–29] provides a simple and efficient method to calculate a local approximation of these forces. Employing this theory entails the depiction of the swimmers' configurations and the computation of their velocity relative to the ambient fluid, necessitating a kinematic formulation as the initial step in addressing the problem.

A. Kinematics

We consider two swimmers, each comprising three rigid links of length L with hinged joints at their ends, moving in the plane defined by the unit vectors $\mathbf{e}_x$ and $\mathbf{e}_y$ (see Fig. 1). In the following, the subscript $i = 1, 2$ denotes the specific microswimmer, while the superscript $j = -1, 0, 1$ identifies its links. More precisely, $j = 0$ represents the central link and $j = -1, 1$ correspond to the adjacent links.

Let $\mathbf{x}_i(t)$ denote the position of the midpoint of the central link of the ith microswimmer:

$$\mathbf{x}_i(t) := \begin{bmatrix} x_i(t) \\ y_i(t) \end{bmatrix}, \quad i = 1, 2, \tag{1}$$

while $\vartheta_i(t)$ denotes the time-dependent angle that the central link forms with the positive x axis. Then, the directions in the plane of each link can be described by the in-plane unit vectors,

$$\mathbf{e}_i^{(j)}(t) := (-1)^{(j)} \begin{bmatrix} \cos\left[\vartheta_i(t) - j\sigma_i^{(j)}(t)\right] \\ \sin\left[\vartheta_i(t) - j\sigma_i^{(j)}(t)\right] \end{bmatrix}, \tag{2}$$

where $\sigma_i^{(j)}(t)$ $(j = -1, 1)$ are angles between successive links, as shown in Fig. 1. Thus the triple $[x_i(t), y_i(t), \vartheta_i(t)]^{\mathrm{T}}$ describes the position and orientation of the ith microswimmer in the plane, while the couple $[\sigma_i^{(-1)}(t), \sigma_i^{(1)}(t)]^{\mathrm{T}}$ describes its *shape*.

We introduce the time-dependent position of a point $\mathbf{x}_i^{(j)}(s, t)$ on the jth link of the ith microswimmer:

$$\mathbf{x}_i^{(j)}(s, t) := \mathbf{x}_i(t) + j\frac{L}{2}\mathbf{e}_i^{(0)}(t) + \left(s + j\frac{L}{2}\right)\mathbf{e}_i^{(j)}(t), \tag{3}$$

where $s \in [-L/2, L/2]$ represents the oriented arc length on each link, following the directions $\mathbf{e}_i^{(j)}(t)$. The velocity of the point $\mathbf{x}_i^{(j)}(s, t)$ is then obtained by direct differentiation of Eq. (3), leading to

$$\mathbf{v}_i^{(j)}(s, t) = \dot{\mathbf{x}}_i(t) + j\frac{L}{2}\mathbf{n}_i^{(0)}(t)\dot{\vartheta}_i(t) + \left(s + j\frac{L}{2}\right)\mathbf{n}_i^{(j)}(t)\left[\dot{\vartheta}_i(t) - j\dot{\sigma}_i^{(j)}(t)\right], \tag{4}$$

where $\mathbf{n}_i^{(j)}(t)$ is the unit vector of the plane $x - y$ perpendicular to $\mathbf{e}_i^{(j)}(t)$: $\mathbf{n}_i^{(j)}(t) := \mathbf{e}_z \times \mathbf{e}_i^{(j)}(t)$.

B. Hydrodynamic force and torque

The calculation of the hydrodynamic interaction is based on the results of Ref. [29], which rely on some specific assumptions reported in the following remark.

Remark 1. We make the same assumptions as in Refs. [23,29], namely that the thickness a of the links is much smaller than the distance h between the swimmers, which is much smaller than their length L,

$$a \ll h \ll L, \tag{5}$$

and that the two microswimmers are approximately straight and nearly parallel to each other:

$$\sigma_i^j \approx \pi, \quad i = 1, 2, \quad j = -1, 1. \tag{6}$$

These assumptions are crucial for applying the force approximation proposed in Ref. [29] to account for the interaction forces between the swimmers.

Let $\mathbf{f}_i^{(j)}(s, t)$ denote the hydrodynamic force density (per unit of length) acting on the point $\mathbf{x}_i^{(j)}(s, t)$. According to resistive force theory [27,29], we take

$$\mathbf{f}_i^{(j)}(s, t) = -\frac{1}{\Lambda}\mathbf{J}_i^{(j)}(t)\mathbf{v}_i^{(j)}(s, t) + \frac{\lambda}{\Lambda}\mathbf{J}_{-i}^{(j)}(t)\mathbf{v}_{-i}^{(j)}(s, t), \tag{7}$$

where $\neg i := 3 - i$, $\lambda(s,t) := \frac{\ln[h(s,t)/L]}{\ln(a/L)} \in (0,1)$, and $\Lambda := 1 - \lambda^2$. The second-order tensor $\mathbf{J}_i^{(j)}(t)$ represents the resistive-force theory operator defined as

$$\mathbf{J}_i^{(j)}(t) := C_\perp \mathbf{I} + C_a \mathbf{E}_i^{(j)}(t), \tag{8}$$

where $\mathbf{E}_i^{(j)}(t) := \mathbf{e}_i^{(j)}(t) \otimes \mathbf{e}_i^{(j)}(t)$ and $C_a = C_\parallel - C_\perp > 0$ denotes the drag anisotropy coefficient, with $C_\perp$ and $C_\parallel > 0$ being the drag coefficients for motion in the direction perpendicular and parallel to the local tangent. Notice that the simplified resistance relation of hydrodynamic interaction in (7) has been tested in Ref. [29] by comparing to more accurate numerical solutions and qualitative agreement has been found.

Henceforth, assuming the proximity of the swimmers as described in Ref. [23], we shall consider the interaction between the jth link of each microswimmer with the jth link of the other microswimmer, while disregarding its interaction with $\neg j$th links.

Remark 2. As stated in Ref. [23], consistent with Eq. (6) and given that we focus on the interaction between corresponding links, it is reasonable to assume that $h = h(s,t)$ remains independent of the spatial variable s and undergoes minimal changes over time. Consequently, it can be treated as a constant, as well as λ.

The hydrodynamic force acting on the ith microswimmer is

$$\mathbf{F}_i(t) = \sum_{j=-1}^{1} \int_{-\frac{L}{2}}^{\frac{L}{2}} \mathbf{f}_i^{(j)}(s,t)\mathrm{d}s, \tag{9}$$

whence, by using (7), we get the linear form

$$\begin{aligned}\mathbf{F}_i(t) = &-\frac{1}{\Lambda}[\mathbf{A}_i(t)\dot{\mathbf{x}}_i(t) + \mathbf{b}_i(t)\dot{\vartheta}_i(t) + \boldsymbol{\alpha}_i(t)\dot{\boldsymbol{\sigma}}_i(t)] \\ &+ \frac{\lambda}{\Lambda}[\mathbf{A}_{\neg i}(t)\dot{\mathbf{x}}_{\neg i}(t) + \mathbf{b}_{\neg i}(t)\dot{\vartheta}_{\neg i}(t) + \boldsymbol{\alpha}_{\neg i}(t)\dot{\boldsymbol{\sigma}}_{\neg i}(t)],\end{aligned} \tag{10}$$

where we have set $\dot{\boldsymbol{\sigma}}_i(t) := [\dot{\sigma}_i^{(-1)}(t), \dot{\sigma}_i^{(1)}(t)]^{\mathrm{T}}$. The details of this calculation and the definitions of $\mathbf{A}$, $\mathbf{b}$, and $\boldsymbol{\alpha}$ can be found in Appendix A.

Similarly, we can calculate the hydrodynamic torque, with respect to the $\mathbf{x}_i(t)$ point, acting on each microswimmer:

$$\mathbf{M}_i(t) = \sum_{j=-1}^{1} \int_{-\frac{L}{2}}^{\frac{L}{2}} \left[\mathbf{x}_i^{(j)}(s,t) - \mathbf{x}_i(t)\right] \times \mathbf{f}_i^{(j)}(s,t)\mathrm{d}s, \tag{11}$$

which is orthogonal to the plane. Thus, by denoting $M_i(t) = \mathbf{M}_i(t) \cdot \mathbf{e}_z$, we obtain

$$\begin{aligned}M_i(t) = &-\frac{1}{\Lambda}[\mathbf{b}_i(t) \cdot \dot{\mathbf{x}}_i(t) + \omega_i(t)\dot{\vartheta}_i(t) + \boldsymbol{\gamma}_i(t)\dot{\boldsymbol{\sigma}}_i(t)] \\ &+ \frac{\lambda}{\Lambda}[\mathbf{d}_i(t) \cdot \dot{\mathbf{x}}_{\neg i}(t) + \bar{\omega}_i(t)\dot{\vartheta}_{\neg i}(t) + \bar{\boldsymbol{\gamma}}_{\neg i}(t)\dot{\boldsymbol{\sigma}}_{\neg i}(t)].\end{aligned} \tag{12}$$

For a more detailed explanation and the definitions of the functions presented in Eq. (12), we again refer the reader to Appendix A.

C. Equations of motion

At low Reynolds numbers, the inertial terms are negligible. Thus the equations of motion simplify to the requirement that the force and torque vanish for each microswimmer:

$$\begin{aligned}\mathbf{F}_i(t) &= \mathbf{0}, \\ M_i(t) &= 0, \quad i = 1, 2.\end{aligned} \tag{13}$$

Using Eqs. (10) and (12), equations of motion can be recast in the form

$$\mathcal{R}(t,\lambda)\begin{bmatrix}\dot{\mathbf{x}}_1(t) \\ \dot{\vartheta}_1(t) \\ \dot{\mathbf{x}}_2(t) \\ \dot{\vartheta}_2(t)\end{bmatrix} + \boldsymbol{\varphi}(t)\begin{bmatrix}\dot{\boldsymbol{\sigma}}_1(t) \\ \dot{\boldsymbol{\sigma}}_2(t)\end{bmatrix} = \mathbf{0}, \tag{14}$$

involving the 6×6 matrix

$$\mathcal{R}(t,\lambda) := \begin{bmatrix}\mathbf{A}_1(t) & \mathbf{b}_1(t) & -\lambda\mathbf{A}_2(t) & -\lambda\mathbf{b}_2(t) \\ \mathbf{b}_1(t)^{\mathrm{T}} & \omega_1(t) & -\lambda\mathbf{d}_1(t) & -\lambda\bar{\omega}_1(t) \\ -\lambda\mathbf{A}_1(t) & -\lambda\mathbf{b}_1(t) & \mathbf{A}_2(t) & \mathbf{b}_2(t) \\ -\lambda\mathbf{d}_2(t) & -\lambda\bar{\omega}_2(t) & \mathbf{b}_2(t)^{\mathrm{T}} & \omega_2(t)\end{bmatrix}, \tag{15}$$

named *the grand resistance matrix*, and the 6×4 matrix

$$\boldsymbol{\varphi}(t) := \begin{bmatrix}\boldsymbol{\alpha}_1(t) & -\lambda\boldsymbol{\alpha}_2(t) \\ \boldsymbol{\gamma}_1(t) & -\lambda\boldsymbol{\gamma}_2(t) \\ -\lambda\boldsymbol{\alpha}_1(t) & \boldsymbol{\alpha}_2(t) \\ -\lambda\boldsymbol{\gamma}_1(t) & \boldsymbol{\gamma}_2(t)\end{bmatrix}.$$

In reformulating the equations of motion into the form (14), we have distinguished the resistive part (first term) from the propulsive part (second term). This separation was made to treat the system as a control system. Indeed, the four angular velocities $\dot{\sigma}_i^{(j)}(t)$ should be considered as gait control functions, which drive the motion of the swimmers. Therefore, by defining $[\dot{\boldsymbol{\sigma}}_1(t), \dot{\boldsymbol{\sigma}}_2(t)]^{\mathrm{T}} =: [\mathbf{u}_1(t), \mathbf{u}_2(t)]^{\mathrm{T}}$, Eq. (14) can be rewritten as

$$\begin{bmatrix}\mathcal{R}(t,\lambda) & \mathbf{0}_{6\times4} \\ \mathbf{0}_{4\times6} & \mathbf{I}_{4\times4}\end{bmatrix}\begin{bmatrix}\dot{\mathbf{x}}_1(t) \\ \dot{\vartheta}_1(t) \\ \dot{\mathbf{x}}_2(t) \\ \dot{\vartheta}_2(t) \\ \dot{\boldsymbol{\sigma}}_1(t) \\ \dot{\boldsymbol{\sigma}}_2(t)\end{bmatrix} = -\begin{bmatrix}\boldsymbol{\varphi}(t) \\ \mathbf{I}_{4\times4}\end{bmatrix}\begin{bmatrix}\mathbf{u}_1(t) \\ \mathbf{u}_2(t)\end{bmatrix}. \tag{16}$$

Then, taking into account the invertibility of the matrix $\mathcal{R}(t,\lambda)$ (see Appendix B), Eq. (16) reduces to

$$\begin{aligned}\begin{bmatrix}\dot{\mathbf{x}}_1(t) \\ \dot{\vartheta}_1(t) \\ \dot{\mathbf{x}}_2(t) \\ \dot{\vartheta}_2(t) \\ \dot{\boldsymbol{\sigma}}_1(t) \\ \dot{\boldsymbol{\sigma}}_2(t)\end{bmatrix} &= \begin{bmatrix}-\mathcal{R}(t,\lambda)^{-1}\boldsymbol{\varphi}(t) \\ \mathbf{I}_{4\times4}\end{bmatrix}\begin{bmatrix}\mathbf{u}_1(t) \\ \mathbf{u}_2(t)\end{bmatrix} \\ &=: \sum_{k=1}^{4} \mathbf{v}_k[\vartheta_1(t), \vartheta_2(t), \boldsymbol{\sigma}_1(t), \boldsymbol{\sigma}_2(t), \lambda]u_k(t),\end{aligned} \tag{17}$$

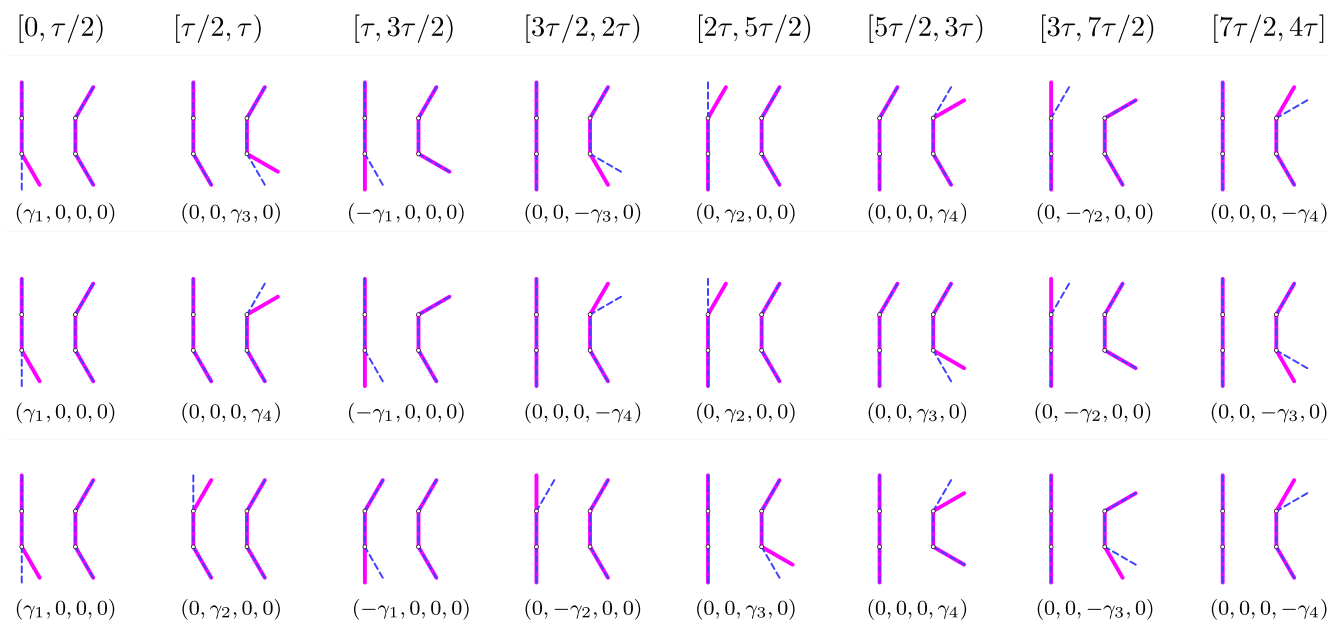

FIG. 2. Schematic representation of the control gaits in a cycle, as described in cases (a) (first line), (b) (second line), and (c) (third line). In each inset, the left swimmer is numbered as *swimmer 1* and the right is numbered as *swimmer 2*. The four-component vector at the bottom of each inset represents the input angular velocities. The solid lines depict the shape of the swimmers at their current configurations, while the dashed lines show their configurations in the previous time step.

where $\mathbf{u}_1(t) = [u_1(t), u_2(t)]^{\mathrm{T}}$ and $\mathbf{u}_2(t) = [u_3(t), u_4(t)]^{\mathrm{T}}$.

In the following, system (17) is analyzed within geometric control theory, by assuming appropriate control gaits $\mathbf{u}_i(t) = \dot{\boldsymbol{\sigma}}_i(t)$ for $i = 1, 2$.

III. LIE BRACKETS ANALYSIS

We now examine the motion of the microswimmers by employing Lie brackets, a classic tool from geometric control theory. For a comprehensive understanding of this theory and its applications, we direct the reader to the book in [30].

We investigate the dynamics of microswimmers when they are nearly straight and nearly parallel to each other, focusing on the interplay of their hydrodynamic interactions. Additionally, we assume that the swimmers' shapes conform to periodic control gaits, as described in Secs. III A and III B, producing small deformations of the swimmers. Furthermore, we assume the initial conditions

$$\vartheta_i^o = \vartheta^o, \quad \boldsymbol{\sigma}_1^o = \begin{bmatrix} \pi \\ \pi \end{bmatrix}, \quad \boldsymbol{\sigma}_2^o = \begin{bmatrix} \pi + \varepsilon\varphi \\ \pi + \varepsilon\varphi \end{bmatrix}, \tag{18}$$

where $\varepsilon \ll 1$ is a small dimensionless parameter and φ is a phase shift. Therefore, swimmers start perfectly aligned only when $\varphi = 0$.

Due to this choice of initial conditions, both swimmers share the same mean orientation, ϑ^o. It is noteworthy that, in this specific instance, Eqs. (17) can be rewritten as

$$\begin{bmatrix} \dot{\mathbf{x}}_1(t) \\ \dot{\vartheta}_1(t) \\ \dot{\mathbf{x}}_2(t) \\ \dot{\vartheta}_2(t) \\ \dot{\boldsymbol{\sigma}}_1(t) \\ \dot{\boldsymbol{\sigma}}_2(t) \end{bmatrix} = \begin{bmatrix} R(\vartheta^o) & \mathbf{0}_{3\times3} & \mathbf{0}_{3\times4} \\ \mathbf{0}_{3\times3} & R(\vartheta^o) & \mathbf{0}_{3\times4} \\ \mathbf{0}_{4\times3} & \mathbf{0}_{4\times3} & \mathbf{I}_{4\times4} \end{bmatrix} \times \sum_{k=1}^{4} \mathbf{v}_k[\boldsymbol{\sigma}_1(t), \boldsymbol{\sigma}_2(t), \lambda] u_k(t), \tag{19}$$

where $R(\vartheta^o)$ is the matrix representing the planar rotation of ϑ^o. This highlights that the system exhibits rototranslation invariance.

A. Nonsimultaneous control gaits

Let us examine the input gait cycle, which consists of eight time subintervals, each spanning $\tau/2$. During each of these subintervals, only one of the two swimmers performs a single action at an assigned angular velocity $\gamma_k > 0$ ($k = 1, 2, 3, 4$). In reference to Fig. 2, subscripts 1 and 3 (2 and 4, respectively) refer to the lower (upper, respectively) links of the left and right swimmers, respectively.

Figure 2 depicts three distinct approaches to assigning control gaits, one for each line (which will be thoroughly examined later), across the eight time subintervals that comprise the control cycle. The four-element vector at the base

of each inset depicts the input angular velocities within a given interval. Below there is the description of the inputs considered.

(a) During the first half of the cycle, the swimmers only move their lower links, while in the second half, they only move their upper links. The swimmers alternate in performing a single action during each interval (Fig. 2, first line).

(b) The two swimmers alternate in their movements, performing opposite strokes in consecutive intervals, i.e., the movement of the lower link of *swimmer 1* is always followed by the movement of the upper link of *swimmer 2* and vice versa (Fig. 2, second line).

(c) In the first half of the cycle, *swimmer 1* undergoes periodic shape changes while *swimmer 2* remains passive. In the second half, the roles of the swimmers are reversed (Fig. 2, third line).

Each case results in distinct displacements, which can be determined by an appropriate combination of the time-dependent vectors $\{\mathbf{v}_1, \ldots, \mathbf{v}_4\}$.

1. Cases (a) and (b)

Let us simplify the notation by defining

$$\mathcal{S}^T(t) := [\mathbf{x}_1(t), \vartheta_1(t), \mathbf{x}_2(t), \vartheta_2(t), \boldsymbol{\sigma}_1(t), \boldsymbol{\sigma}_2(t)]^T$$

and

$$\Upsilon := \mathcal{S}(4\tau) - \mathcal{S}(0), \tag{20}$$

which represents the change of state after a cycle.

We note that Υ has six nonzero entries. When the control gaits are those of cases (a) and (b), the calculation of Lie brackets, up to $O((\gamma_i\tau)^2)$, yields

$$\Upsilon^{(a)} = \frac{\tau^2}{4}\gamma_1\gamma_3\mathbf{w}^o_{13}(\boldsymbol{\sigma}^o_1, \boldsymbol{\sigma}^o_2, \vartheta^o) + \frac{\tau^2}{4}\gamma_2\gamma_4\mathbf{w}^o_{24}(\boldsymbol{\sigma}^o_1, \boldsymbol{\sigma}^o_2, \vartheta^o), \tag{21a}$$

$$\Upsilon^{(b)} = \frac{\tau^2}{4}\gamma_1\gamma_4\mathbf{w}^o_{14}(\boldsymbol{\sigma}^o_1, \boldsymbol{\sigma}^o_2, \vartheta^o) + \frac{\tau^2}{4}\gamma_2\gamma_3\mathbf{w}^o_{23}(\boldsymbol{\sigma}^o_1, \boldsymbol{\sigma}^o_2, \vartheta^o), \tag{21b}$$

respectively, where $\mathbf{w}^o_{hk}$ $(h, k = 1, 2, 3, 4)$ denotes the Lie bracket:

$$\mathbf{w}^o_{hk}(\boldsymbol{\sigma}^o_1, \boldsymbol{\sigma}^o_2, \vartheta^o) := [\mathbf{v}_h, \mathbf{v}_k]|_{(\boldsymbol{\sigma}^o_1, \boldsymbol{\sigma}^o_2)}. \tag{22}$$

Remark 3. Note that on the one hand we have chosen constant inputs γ_i and on the other hand we require the maximum angular amplitude to be $\varepsilon\varphi$. This necessarily implies that $\gamma_i\tau$ is $O(\varepsilon)$; therefore, we use the following notation: $\mathbf{w}^o_{hk}(\boldsymbol{\sigma}^o_1, \boldsymbol{\sigma}^o_2, \vartheta^o) = \mathbf{w}^o_{hk}(\varphi, \vartheta^o)$.

From Remark 3, we expect the components of the displacement $\Upsilon^{(a)}$ and $\Upsilon^{(b)}$ to be at least $O(\varepsilon^4)$. However, explicit calculations reveal that $\Upsilon^{(a)}$ and $\Upsilon^{(b)}$ are $O(\varepsilon^5)$. Thus we conclude that the considered control gaits lead to negligible displacements and/or rotations of the two microswimmers.

2. Case (c)

In this case, calculations of Lie brackets up to $O((\gamma_i\tau)^2)$ result in

$$\Upsilon^{(c)} = \frac{\tau^2}{4}\gamma_1\gamma_2\mathbf{w}^o_{12}(\varphi, \vartheta^o) + \frac{\tau^2}{4}\gamma_3\gamma_4\mathbf{w}^o_{34}(\varphi, \vartheta^o). \tag{23}$$

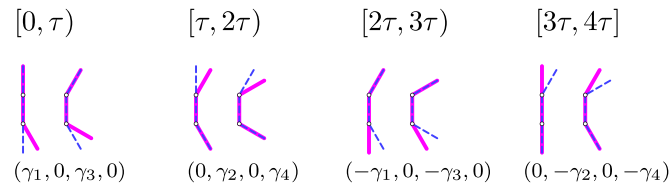

FIG. 3. Sketch of two Purcell swimmers beating simultaneously. A swimming cycle consists of four phases in which the swimmers perform simultaneous movements. The solid lines represent the current shape of the swimmers, while the dashed lines depict their shape in the previous time step.

Assuming for simplicity $\gamma_i = \gamma$ $(i = 1, 2, 3, 4)$ and $C_\perp = 2C_\parallel$ [25], the nonzero entries of $\Upsilon^{(c)}$ become

$$\Upsilon^{(c)}_1(\varphi, \vartheta^o) = q_1(\varphi)\cos\vartheta^o, \tag{24a}$$

$$\Upsilon^{(c)}_2(\varphi, \vartheta^o) = q_1(\varphi)\sin\vartheta^o, \tag{24b}$$

$$\Upsilon^{(c)}_3(\varphi) = \frac{\varepsilon^3}{4}\left(\frac{2(-5+\lambda)\lambda\varphi}{729(\lambda^2-1)}\right), \tag{24c}$$

$$\Upsilon^{(c)}_4(\varphi, \vartheta^o) = q_2(\varphi)\cos\vartheta^o, \tag{24d}$$

$$\Upsilon^{(c)}_5(\varphi, \vartheta^o) = q_2(\varphi)\sin\vartheta^o, \tag{24e}$$

$$\Upsilon^{(c)}_6(\varphi) = \frac{\varepsilon^3}{4}\left(\frac{2(-45+\lambda+40\lambda^2)\varphi}{729(\lambda^2-1)}\right), \tag{24f}$$

with

$$q_1(\varphi) := L\frac{\varepsilon^4}{4}\left(-\frac{5}{81} + \frac{10\lambda^2\varphi^2}{2187(\lambda^2-1)}\right),$$

$$q_2(\varphi) := L\frac{\varepsilon^4}{4}\left(\frac{2(-245-\lambda+238\lambda^2)\varphi^2}{2187(\lambda^2-1)} - \frac{5}{81}\right).$$

Since $\Upsilon^{(c)}$ is $O(\varepsilon^4)$, we safely neglect $\Upsilon^{(a)}$ and $\Upsilon^{(b)}$, both of which are $O(\varepsilon^5)$. Furthermore, the presence of ϑ^o in the first, second, fourth, and fifth components indicates that the system moves in the direction of the main orientation of both swimmers.

Finally, we emphasize that all the components of the Lie brackets, for this case and for the next cases to be developed, depend on the drag coefficients only through their ratio $C_\parallel/C_\perp$. For brevity of the formulas, we have assumed $C_\parallel/C_\perp = 2$, as indicated in Ref. [27].

B. Simultaneous control gaits

This section focuses on numerical results for the case of equal simultaneous control gaits. The periodic loop of both swimmers has been partitioned into four temporal subintervals; during each subinterval, the swimmers move the adjacent links simultaneously, i.e., the upper or lower links in pairs. Figure 3 depicts a sketch of this case.

Under these conditions, up to $O((\gamma_i\tau)^2)$, Lie bracket analysis yields

$$\Upsilon^{(S)} = \tau^2\big[\gamma_1\gamma_2\mathbf{w}^o_{12}(\varphi, \vartheta^o) - \gamma_2\gamma_3\mathbf{w}^o_{23}(\varphi, \vartheta^o) + \gamma_1\gamma_4\mathbf{w}^o_{14}(\varphi, \vartheta^o) + \gamma_3\gamma_4\mathbf{w}^o_{34}(\varphi, \vartheta^o)\big], \tag{25}$$

with $\mathbf{w}^o_{hk}$ defined as in (22).

To facilitate the discussion, let us focus on the specific instance where the links rotate with the same angular velocity:

$$\gamma_i = \gamma, \quad i = 1, \dots, 4.$$

Thus Eq. (25) reduces to

$$\Upsilon^{(S)} = \tau^2\gamma^2\mathbf{w}^o(\varphi, \vartheta^o), \tag{26}$$

where

$$\mathbf{w}^o(\varphi, \vartheta^o) = [\mathbf{s}_1(\cdot, \lambda), \mathbf{s}_2(\cdot, \lambda)]|_{(\boldsymbol{\sigma}_1^0, \boldsymbol{\sigma}_2^0)}, \tag{27}$$

with

$$\mathbf{s}_1(\cdot, \lambda) := \mathbf{v}_1[\boldsymbol{\sigma}_1(t), \boldsymbol{\sigma}_2(t), \lambda] + \mathbf{v}_3[\boldsymbol{\sigma}_1(t), \boldsymbol{\sigma}_2(t), \lambda]$$

and

$$\mathbf{s}_2(\cdot, \lambda) := \mathbf{v}_2[\boldsymbol{\sigma}_1(t), \boldsymbol{\sigma}_2(t), \lambda] + \mathbf{v}_4[\boldsymbol{\sigma}_1(t), \boldsymbol{\sigma}_2(t), \lambda].$$

Details of this calculation can be found in Appendix D.

After some straightforward algebra, we arrive at

$$\Upsilon_1^{(S)}(\varphi, \vartheta^o) = p_1(\varphi)\cos\vartheta^o, \tag{28a}$$

$$\Upsilon_2^{(S)}(\varphi, \vartheta^o) = p_1(\varphi)\sin\vartheta^o, \tag{28b}$$

$$\Upsilon_3^{(S)}(\varphi) = \varepsilon^3\frac{2\lambda\varphi}{81(1+\lambda)}, \tag{28c}$$

$$\Upsilon_4^{(S)}(\varphi, \vartheta^o) = p_2(\varphi)\cos\vartheta^o, \tag{28d}$$

$$\Upsilon_5^{(S)}(\varphi, \vartheta^o) = p_2(\varphi)\sin\vartheta^o, \tag{28e}$$

$$\Upsilon_6^{(S)}(\varphi) = \varepsilon^3\frac{2(45+36\lambda)\varphi}{729(1+\lambda)}, \tag{28f}$$

with

$$p_1(\varphi) := L\varepsilon^4\left(-\frac{5}{81} + \frac{2(5\lambda^2 - 12\lambda)\varphi^2}{2187(\lambda^2-1)}\right),$$

$$p_2(\varphi) := L\varepsilon^4\left(-\frac{5}{81} + \frac{2(-245 - 4\lambda + 242\lambda^2)\varphi^2}{2187(\lambda^2-1)}\right).$$

C. Discussion

According to Eqs. (24) and (28), the nonsimultaneous and simultaneous cases exhibit the following similarities.

(i) Not surprisingly, in the absence of hydrodynamic interaction ($\lambda = 0$), the two swimmers behave as two independent Purcell swimmers, which are individually controllable. Furthermore, as expected, in this limiting condition, the initial misalignment ($\varphi \neq 0$) does not affect the motion.

(ii) Similarly, when the swimmers are initially aligned ($\varphi = 0$) the hydrodynamic interaction plays no role.

(iii) At order $O(\varepsilon^4)$, the swimmers move along their mean common orientation ϑ^o, like two noninteracting Purcell swimmers. This can be seen from the expressions $\Upsilon_1^{(c)}$, $\Upsilon_2^{(c)}$, $\Upsilon_4^{(c)}$, $\Upsilon_5^{(c)}$ and $\Upsilon_1^{(S)}$, $\Upsilon_2^{(S)}$, $\Upsilon_4^{(S)}$, $\Upsilon_5^{(S)}$.

(iv) Hydrodynamic interaction induces reorientation when $\varphi \neq 0$ of the central link of both swimmers of order $O(\varepsilon^3)$, as can be seen from expressions $\Upsilon_3^{(c)}$, $\Upsilon_6^{(c)}$ and $\Upsilon_3^{(S)}$, $\Upsilon_6^{(S)}$. There is no such reorientation in the case $\varphi = 0$.

To determine which of the two cases is more effective, we determine the midpoint of the points $\mathbf{x}_1(t)$ and $\mathbf{x}_2(t)$:

$$\mathbf{x}_m(t) := \frac{\mathbf{x}_1(t) + \mathbf{x}_2(t)}{2}.$$

Then, denoting $\Delta\mathbf{x}_m := \mathbf{x}_m(4\tau) - \mathbf{x}_m^o$ the displacement of $\mathbf{x}_m$ at the end of a swimming loop, up to $O(\varepsilon^4)$, we get

$$\Delta\mathbf{x}_m^{(c)} = \frac{\varepsilon^4}{4}[q_1(\varphi) + q_2(\varphi)]\begin{bmatrix}\cos\vartheta^o\\ \sin\vartheta^o\end{bmatrix}, \tag{29a}$$

$$\Delta\mathbf{x}_m^{(S)} = \varepsilon^4[p_1(\varphi) + p_2(\varphi)]\begin{bmatrix}\cos\vartheta^o\\ \sin\vartheta^o\end{bmatrix}, \tag{29b}$$

for the nonsimultaneous and simultaneous cases, respectively, whence

$$\left|\Delta\mathbf{x}_m^{(c)}\right| = \frac{L\varepsilon^4}{4}\left[\frac{5}{81} - \frac{(-245 - \lambda + 243\lambda^2)}{2187(\lambda^2-1)}\varphi^2\right], \tag{30a}$$

$$\left|\Delta\mathbf{x}_m^{(S)}\right| = \frac{L\varepsilon^4}{81}\left[5 - \frac{247\lambda^2 - 16\lambda - 245}{27(\lambda^2-1)}\varphi^2\right]. \tag{30b}$$

Therefore, we get

$$\left|\Delta\mathbf{x}_m^{(S)}\right| - \left|\Delta\mathbf{x}_m^{(c)}\right| = \frac{L\varepsilon^4}{8748(\lambda^2-1)}[\lambda^2(405 - 745\varphi^2) + 63\lambda\varphi^2 - 405 + 735\varphi^2] > 0,$$

for $\lambda \in (0, 1)$, and $\varepsilon \ll 1$, which leads us to the conclusion that simultaneous control gaits are more efficient than nonsimultaneous control gaits.

Finally, a glance at Eq. (30b) shows that, since

$$\frac{247\lambda^2 - 16\lambda - 245}{2187(\lambda^2-1)}\varphi^2 > 0, \quad \lambda \in (0, 1),$$

the greater the alignment between the swimmers, i.e., φ decreasing, the greater their displacement. Therefore, swimming in phase is more efficient. This agrees with the phase locking phenomenon reported in Ref. [25]. Moreover, the interaction reduces the performance of the two swimmers, since at a fixed φ, $|\Delta\mathbf{x}_m^{(S)}|$ is a decreasing function of λ (see Fig. 9).

Remark 4. The motivation behind employing piecewise constant controls in the discussed scenarios lies primarily in the desire to simplify computations. Nonetheless, the direct proportionality of the outputs $\Upsilon^{(a)}$, $\Upsilon^{(b)}$, $\Upsilon^{(c)}$, and $\Upsilon^{(S)}$ to the Lie brackets of the control vector fields stems solely from the utilization of periodic controls, not the specific choice of piecewise constant controls. It is well documented in Refs. [31–34] that any non-self-intersecting periodic control loop will result in a state change that is directly proportional to the Lie brackets of the control vector fields after a single cycle. Accordingly, we have opted for the simplest control loop that achieves the desired state change, namely, the rectangular loop with sides γ_i.

IV. NUMERICAL SIMULATIONS

This section is devoted to numerical results for the case of equal simultaneous control gaits, as illustrated in Fig. 3, which represent the most efficient case among those analyzed through Lie brackets analysis. We chose the control gaits as piecewise constant functions, with $\gamma_i = \gamma$ for

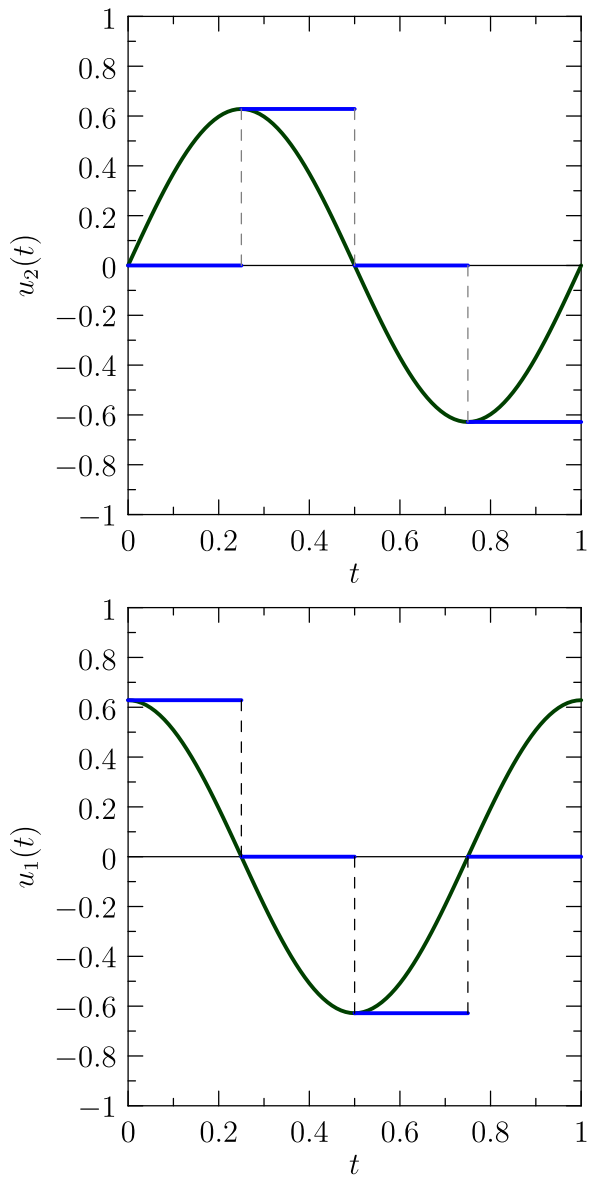

FIG. 4. Piecewise constant (blue lines) and smooth continuous (dark green continuous lines) input angular velocities for the upper (upper figure) and lower (lower figure) links.

$i = 1, \ldots, 4$ (Fig. 4, blue lines) and we solve the system of equations (17) with the parameter values as in Table I, according to Refs. [23,29]. We demonstrate that the numerical results are in concordance with the findings obtained from Lie bracket analysis.

We commence our examination by evaluating two distinct types of control gaits, as shown in Fig. 4—namely, the

TABLE I. Values of the parameters used in numerical simulations.

τ	γ	L	λ	$C_\perp$	$C_\parallel$	ϑ^o
0.25 s	0.63 s^{-1}	1 μm	0.62	1 Ns/μm^2	2 Ns/μm^2	$\pi/2$

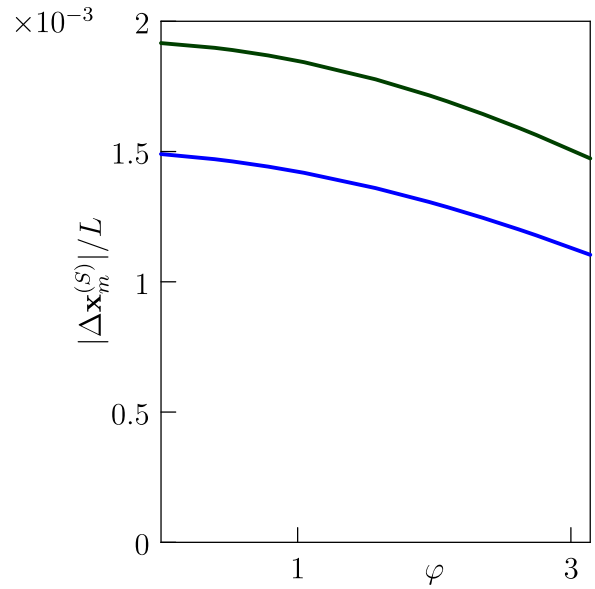

FIG. 5. Dimensionless numerical displacement $|\Delta \mathbf{x}_m^{(S)}|/L$ in a cycle corresponding to piecewise constant gaits [blue (lower) line] and continuous gaits [green (upper) line].

piecewise constant functions

$$u_1(t) = \begin{cases} \gamma & \text{for } 0 \leqslant t \leqslant \tau, \\ 0 & \text{for } \tau \leqslant t \leqslant 2\tau, \\ -\gamma & \text{for } 2\tau \leqslant t \leqslant 3\tau, \\ 0 & \text{for } 3\tau \leqslant t \leqslant 4\tau, \end{cases}$$

$$u_2(t) = \begin{cases} 0 & \text{for } 0 \leqslant t \leqslant \tau, \\ \gamma & \text{for } \tau \leqslant t \leqslant 2\tau, \\ 0 & \text{for } 2\tau \leqslant t \leqslant 3\tau, \\ -\gamma & \text{for } 3\tau \leqslant t \leqslant 4\tau, \end{cases}$$

and the sinusoidal continuous functions,

$$u_1(t) = \gamma \cos(\omega t), \quad u_2(t) = \gamma \sin(\omega t), \quad \omega = \frac{\pi}{2\tau} = \frac{\gamma}{\varepsilon}.$$

These inputs have been carefully adjusted to deliver the same maximum angular amplitude and maintain phase concordance.

The dimensionless displacement $|\Delta \mathbf{x}_m^{(S)}|/L$ as a function of the displacement angle φ for $\varepsilon = 0.1$ is shown in Fig. 5. The qualitative agreement between the two curves provides support for Remark 4, allowing us to proceed with our analysis by solely examining piecewise constant gaits, for which we have already obtained analytical results in the previous section.

Figure 6 illustrates the theoretical (red dashed line) and the numerical dimensionless displacement (solid blue line) as a function of the angle φ, for $\varepsilon = 0.1$. Within the analytical approximation, the curves demonstrate remarkable agreement, revealing that the displacement diminishes with increasing displacement angle. Consequently, we can infer that the maximum displacement is achieved at $\varphi = 0$, implying that the microswimmers attain their peak performance when they beat in phase. Finally, Fig. 7 shows the variation of the relative

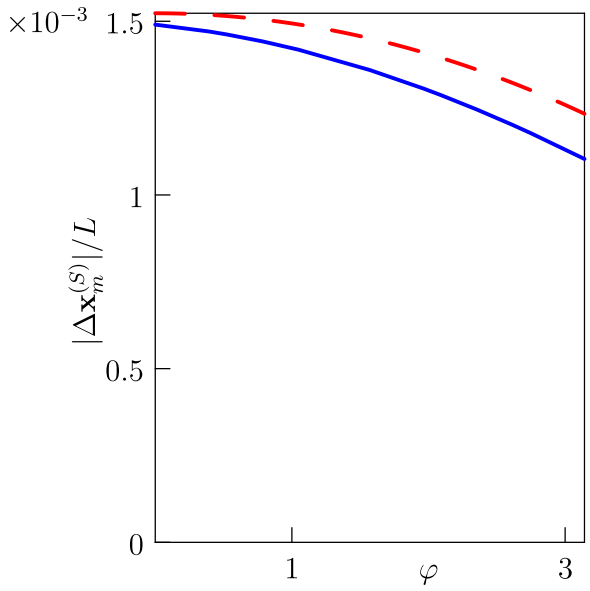

FIG. 6. Theoretical (dashed line) and numerical (solid line) dimensionless displacement $|\Delta\mathbf{x}_m^{(S)}|/L$ as a function of φ, using the parameters as reported in Table I and $\varepsilon = 0.1$.

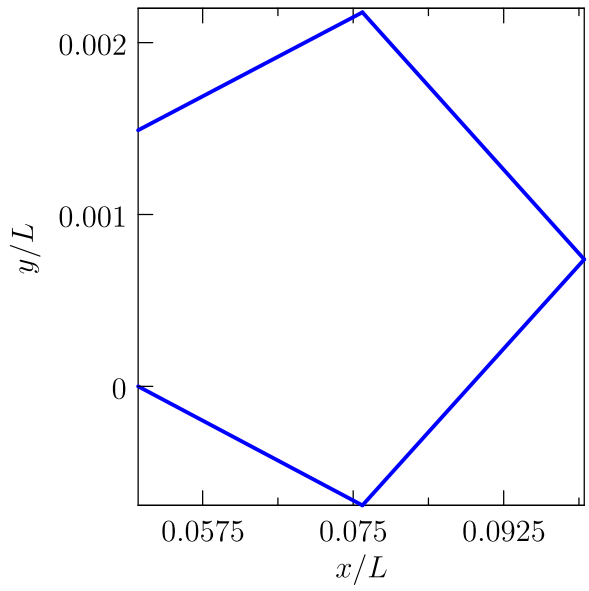

FIG. 8. Trajectory of the midpoint $\mathbf{x}_m(t)$ in a cycle, obtained by numerical simulations. The parameters are chosen as in Table I, $\varphi = 0$ and $\varepsilon = 0.1$.

error, defined as

$$\mathrm{err_r} := \left| \frac{\left|\Delta\mathbf{x}_\mathrm{m}^{(\mathrm{S})}\right| - \left|\Delta\mathbf{x}_\mathrm{m}^{(\mathrm{S})}\right|_\mathrm{num}}{\left|\Delta\mathbf{x}_\mathrm{m}^{(\mathrm{S})}\right|_\mathrm{num}} \right|, \tag{31}$$

depends on ε. Here $|\Delta\mathbf{x}_m^{(S)}|_\mathrm{num}$ represents the displacement obtained from numerical integration.

To visualize the movement of the two-swimmer system throughout a cycle, Fig. 8 depicts the numerical trajectory of the midpoint $\mathbf{x}_m(t)$, for $\varphi = 0$ and $\varepsilon = 0.1$. The swimmers exhibit a significant lateral shift to propel themselves in the longitudinal direction. However, in line with the theoretical analysis [see Eqs. (28) when $\vartheta^o = \pi/2$], the overall displacement after a cycle occurs along the y axis.

It is crucial to note that, for $\varphi = 0$, Eq. (30b) indicates that the displacement does not depend on λ. In this instance, the hydrodynamic interaction between the swimmers does not influence the system's displacement and it is identical to that of a single swimmer under the same control conditions [31].

Influence of the parameter λ

The parameter $\lambda \in [0, 1)$ represents the strength of the hydrodynamic interaction between the two microswimmers.

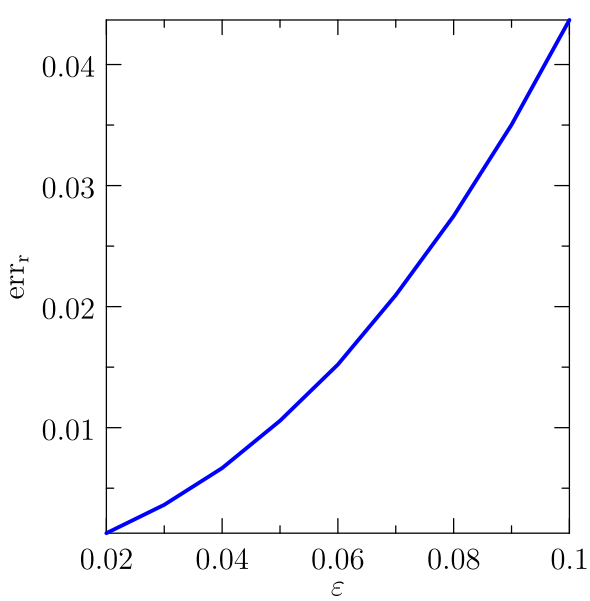

FIG. 7. Function err [defined in (31)] vs ε. We have set $\varphi = \pi/4$ and $\lambda = 0.6$.

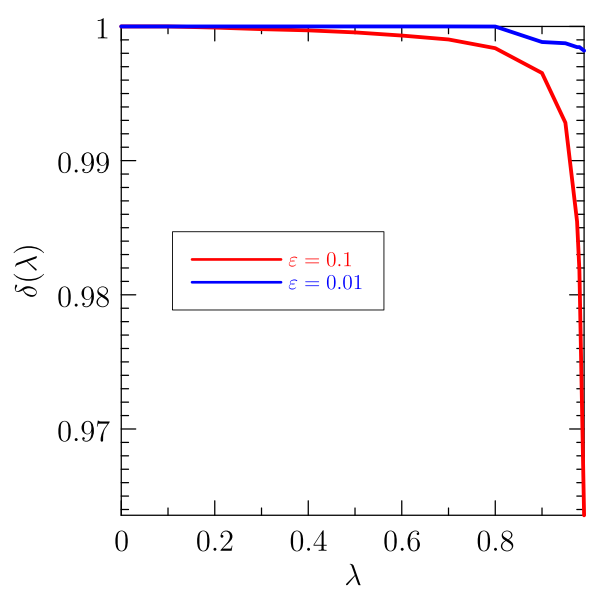

FIG. 9. $\delta(\lambda)$ as a function of λ, for $\varphi = \frac{\pi}{4}$ and $\varepsilon = 0.1, 0.01$. The parameters L, $C_\parallel$, and $C_\perp$ were chosen as in Table I.

As Eqs. (10) and (15) indicate, the limit $\lambda \to 0$ represents the absence of hydrodynamic interaction. Consequently, equations of motion (14) decouple and become those of two noninteracting microswimmers.

It should be noted that the limit $\lambda \to 0$ can be reached in two distinct ways: first, the distance h between the swimmers approaches the length of a link L, which clearly violates the limit (5); second, in the limit of vanishing thickness, where $a \to 0$.

In contrast, the opposite limit $\lambda \to 1$ is achieved when the thickness a of each swimmer approaches the distance h between them, which again violates limit (5).

As stated in Ref. [27], although Eq. (7) was derived exclusively asymptotically in the limit where $a/h \to 0$ and $h/L \to 0$, it can be seen that even when these parameters are not asymptotically small, Eq. (7) can effectively approximate the computational results. It therefore becomes relevant to investigate how the parameter λ influences the motion of the two swimmers.

To investigate the impact of the interaction parameter λ, we introduce the function

$$\delta(\lambda) := \frac{\left|\Delta \mathbf{x}_m^{(S)}(\lambda)\right|}{\left|\Delta \mathbf{x}_m^{(S)}(0)\right|}, \tag{32}$$

which measures the displacement of two interacting swimmers relative to two noninteracting ones, which is plotted in Fig. 9. Two effects can be inferred: (i) hydrodynamic interaction increases with increasing angular opening of the swim, i.e., for increasing ε; (ii) hydrodynamic interaction hinders the movement of swimmers, inasmuch as, at a fixed value of ε, δ is a decreasing function of λ.

V. CONCLUSIONS

In this study, we derived the equations of motion for two Purcell swimmers that engage in mutual interaction within a viscous fluid. These equations were then presented in the framework of a control system, with the angular velocities of the strokes serving as input parameters, bearing in mind that internal biomechanical actuators drive the swimmers' motion.

To achieve analytical progress and to develop the model within the framework of resistive force theory, we assumed that the two three-link swimmers are approximately straight, parallel to each other, and subject to small deformations.

Through Lie bracket analysis together with numerical results, we deduced that (i) simultaneous swimming is more efficient than nonsimultaneous swimming, (ii) simultaneous swimmers perform better if they are in phase with each other, (iii) fluid-mediated interaction between swimmers hinders their performance, and (iv) swimming simultaneously and in phase is a way for swimmers to overcome the disadvantage caused by hydrodynamic interaction.

Our outcomes match the phase locking phenomena discussed in Refs. [25,26] and Taylor's calculations [35], which indicated that the most energetically advantageous situation occurs when waves moving along the swimmers' flagella travel in phase.

ACKNOWLEDGMENTS

M.Z. and G.N. acknowledge that the present research has been partially supported by PRIN grant *Mathematics for industry 4.0 (Math4I4)* (Grant No. 2020F3NCPX). All authors acknowledge support as members of the Gruppo Nazionale per la Fisica Matematica (GNFM) of the Istituto Nazionale di Alta Matematica (INdAM).

APPENDIX A: HYDRODYNAMIC FORCE AND TORQUE

To supplement Sec. II B, this Appendix derives the equations of motion in detail. We start by substituting the expression of the resistive-force operator, defined by Eq. (8), into Eq. (7), thus obtaining

$$\begin{aligned}\mathbf{f}_i^{(j)}(s,t) = -\frac{1}{\Lambda}\Bigg[&C_\perp \dot{\mathbf{x}}_i(t) + C_\perp j\frac{L}{2}\mathbf{n}_i^{(0)}(t)\dot{\vartheta}_i(t) + C_\perp[\dot{\vartheta}_i(t) - j\dot{\sigma}_i^{(j)}(t)]\left(s + j\frac{L}{2}\right)\mathbf{n}_i^{(j)}(t)\\ &+ C_a\mathbf{E}_i^{(j)}(t)\dot{\mathbf{x}}_i(t) + C_a j\frac{L}{2}\mathbf{E}_i^{(j)}(t)\mathbf{n}_i^{(0)}(t)\dot{\vartheta}_i(t)\Bigg] + \frac{\lambda}{\Lambda}\Bigg[C_\perp\dot{\mathbf{x}}_{\neg i}(t) + C_\perp j\frac{L}{2}\mathbf{n}_{\neg i}^{(0)}(t)\dot{\vartheta}_{\neg i}(t)\\ &+ C_\perp[\dot{\vartheta}_{\neg i}(t) - j\dot{\sigma}_{\neg i}^{(j)}(t)]\left(s + j\frac{L}{2}\right)\mathbf{n}_{\neg i}^{(j)}(t) + C_a\mathbf{E}_{\neg i}^{(j)}(t)\dot{\mathbf{x}}_{\neg i}(t) + C_a j\frac{L}{2}\mathbf{E}_{\neg i}^{(j)}(t)\mathbf{n}_{\neg i}^{(0)}(t)\dot{\vartheta}_{\neg i}(t)\Bigg].\end{aligned} \tag{A1}$$

Then, integration of Eq. (A1) over $s \in [-L/2, L/2]$ yields the time-dependent force acting on the jth link of the ith microswimmer. Finally, for each swimmer, we add together the contributions on the single links:

$$\mathbf{F}_i(t) := \sum_{j=-1}^{1}\int_{-\frac{L}{2}}^{\frac{L}{2}} \mathbf{f}_i^{(j)}(s,t)\mathrm{d}s, \quad i = 1, 2, \tag{A2}$$

yielding Eq. (10), where

$$\mathbf{A}_i(t) := L\big[3C_\perp\mathbf{I} + C_a\big[\mathbf{E}_i^{(-1)}(t) + \mathbf{E}_i^{(0)}(t) + \mathbf{E}_i^{(1)}(t)\big]\big],$$

$$\mathbf{b}_i(t) := \frac{L^2}{2}\big[C_\perp\big(\mathbf{n}_i^{(1)}(t) - \mathbf{n}_i^{(-1)}(t)\big) + C_a\big(\mathbf{E}_i^{(1)}(t) - \mathbf{E}_i^{(-1)}(t)\big)\mathbf{n}_i^{(0)}(t)\big],$$

$$\boldsymbol{\alpha}_i(t) := -\frac{L^2}{2}C_\perp\big[\mathbf{n}_i^{(-1)}(t), \mathbf{n}_i^{(1)}\big]. \tag{A3a}$$

The definitions of $\mathbf{A}_{\neg i}(t)$, $\mathbf{b}_{\neg i}(t)$, and $\boldsymbol{\alpha}_{\neg i}(t)$ can be obtained by Eqs. (A3) provided to replace i by $\neg i$.

To determine the hydrodynamic torque acting on the swimmers, we note that all forces lie within the $x-y$ plane and act on points in the $x-y$ plane. Consequently, the torque density, and thus the torque itself, lies along the z axis.

We use Eqs. (1), (3), and (A1) to determine the density of torque in a point of the jth link of the ith microswimmer:

$$\begin{aligned}
m_i^{(j)}(s,t) &:= \big\{\big[\mathbf{x}_i^{(j)}(s,t) - \mathbf{x}_i(t)\big] \times \mathbf{f}_i^{(j)}(s,t)\big\} \cdot \mathbf{e}_z \\
&= -\frac{1}{\Lambda}\bigg[j\frac{L}{2}C_\perp\big[\mathbf{n}_i^{(0)}(t) + \mathbf{n}_i^{(j)}(t)\big]\dot{\mathbf{x}}_i(t) + j^2\frac{L^2}{4}C_\perp\dot{\vartheta}_i(t)\big[1 + 2\mathbf{n}_i^{(j)}(t)\cdot\mathbf{n}_i^{(0)}(t)\big] + \bigg(j^2\frac{L^2}{4} + s^2\bigg)C_\perp\big[\dot{\vartheta}_i(t) - j\sigma_i^{(j)}(t)\big] \\
&\quad + j\frac{L}{2}C_a\mathbf{n}_i^{(0)}(t)\cdot\mathbf{E}_i^{(j)}(t)\dot{\mathbf{x}}_i(t) + j^2\frac{L^2}{4}C_a\mathbf{n}_i^{(0)}(t)\cdot\mathbf{E}_i^{(j)}(t)\dot{\mathbf{n}}_i^{(0)}(t)\dot{\vartheta}_i(t)\bigg] + \frac{\lambda}{\Lambda}\bigg[j\frac{L}{2}C_\perp[\mathbf{n}_i^{(0)}(t) + \mathbf{n}_i^{(j)}(t)]\dot{\mathbf{x}}_{\neg i}(t) \\
&\quad + j^2\frac{L^2}{4}C_\perp\dot{\vartheta}_{\neg i}(t)\big[\mathbf{n}_i^{(j)}(t) + \mathbf{n}_i^{(0)}(t)\big]\cdot\mathbf{n}_{\neg i}^{(0)}(t) + \bigg(j^2\frac{L^2}{4} + s^2\bigg)C_\perp\big[\dot{\vartheta}_{\neg i}(t) - j\sigma_{\neg i}^{(j)}(t)\big]\big[2\mathbf{n}_i^{(j)}(t) + \mathbf{n}_i^{(0)}(t)\big]\cdot\mathbf{n}_{\neg i}^{(j)} \\
&\quad + j\frac{L}{2}C_a\big[\mathbf{n}_i^{(0)}(t) + \mathbf{n}_i^{(j)}(t)\big]\cdot\mathbf{E}_{\neg i}^{(j)}(t)\dot{\mathbf{x}}_{\neg i}(t) + j^2\frac{L^2}{4}C_a\dot{\vartheta}_{\neg i}(t)\big[\mathbf{n}_i^{(0)}(t) + \mathbf{n}_i^{(j)}(t)\big]\cdot\mathbf{E}_{\neg i}^{(j)}(t)\dot{\mathbf{n}}_{\neg i}^{(0)}(t)\bigg].
\end{aligned} \tag{A4}$$

Note that in writing Eq. (5) we have intentionally omitted the linear terms in s which make no contribution to the total torque.

The total torque acting on the ith swimmer is then

$$M_i(t) := \sum_{j=-1}^{1}\int_{-L/2}^{L/2} m_i^{(j)}(s,t)\mathrm{d}s, \quad i = 1, 2, \tag{A5}$$

which leads to Eq. (12), where

$$\begin{aligned}
\omega_i(t) &:= \frac{5}{4}L^3C_\perp + \frac{L^3}{4}C_a\mathbf{n}_i^{(0)}(t)^{\mathrm{T}}\cdot\big[\mathbf{E}_i^{(1)}(t)\mathbf{E}_i^{(-1)}(t)\big]\cdot\mathbf{n}_i^{(0)}(t) + \frac{L^3}{2}C_\perp\big(\mathbf{n}_i^{(0)}(t)^{\mathrm{T}}\cdot\big[\mathbf{n}_i^{(-1)}(t) + \mathbf{n}_i^{(1)}(t)\big]\big), \\
\boldsymbol{\gamma}_i(t) &= \frac{L^3}{4}C_\perp\big\{\mathbf{n}_i^{(-1)}(t)^{\mathrm{T}}\cdot[\mathbf{n}_i^{(0)}(t) + \mathbf{n}_i^{(-1)}(t)], -\mathbf{n}_i^{(1)}(t)^{\mathrm{T}}\cdot\big[\mathbf{n}_i^{(0)}(t) + \mathbf{n}_i^{(1)}(t)\big]\big\}, \\
\mathbf{d}_i(t) &:= \frac{L^2}{2}C_a\big[\mathbf{n}_i^{(1)}(t)^{\mathrm{T}}\cdot\mathbf{E}_{\neg i}^{(1)}(t) - \mathbf{n}_i^{(-1)}(t)^{\mathrm{T}}\cdot\mathbf{E}_{\neg i}^{(-1)}(t)\big] + \bar{\mathbf{b}}_{\neg i}(t), \\
\bar{\mathbf{b}}_{\neg i}(t) &= \frac{L^2}{2}\big[C_\perp\big(\mathbf{n}_i^{(1)}(t) - \mathbf{n}_i^{(-1)}(t)\big)^{\mathrm{T}} + C_a\big(\mathbf{n}_i^{(0)}(t)^{\mathrm{T}}\cdot[\mathbf{E}_{\neg i}^{(1)}(t) - \mathbf{E}_{\neg i}^{(-1)}(t)]\big)\big],
\end{aligned}$$

$$\begin{aligned}
\bar{\omega}_i(t) &= \frac{7}{12}L^3C_\perp\mathbf{n}_i^{(0)}(t)^{\mathrm{T}}\cdot\mathbf{n}_{\neg i}^{(0)}(t) + \frac{L^3}{4}C_a\mathbf{n}_i^{(0)}(t)^{\mathrm{T}}\cdot\big[\mathbf{E}_{\neg i}^{(1)}(t) + \mathbf{E}_{\neg i}^{(-1)}(t)\big]\cdot\mathbf{n}_{\neg i}^{(0)}(t) \\
&\quad + \frac{L^3}{4}C_\perp\big(\big[\mathbf{n}_i^{(-1)}(t) + \mathbf{n}_i^{(1)}(t)\big]^{\mathrm{T}}\cdot\mathbf{n}_{\neg i}^{(0)}(t) + \mathbf{n}_i^{(0)}(t)^{\mathrm{T}}\cdot\big[\mathbf{n}_{\neg i}^{(1)}(t) + \mathbf{n}_{\neg i}^{(-1)}(t)\big] \\
&\quad + \mathbf{n}_i^{(-1)}(t)^{\mathrm{T}}\cdot\mathbf{n}_{\neg i}^{(-1)}(t) + \mathbf{n}_i^{(1)}(t)^{\mathrm{T}}\cdot\mathbf{n}_{\neg i}^{(1)}(t)\big) + \frac{L^3}{4}C_a\big[\mathbf{n}_i^{(1)}(t)^{\mathrm{T}}\cdot\mathbf{E}_{\neg i}^{(1)}(t) + \mathbf{n}_i^{(-1)}(t)^{\mathrm{T}}\cdot\mathbf{E}_{\neg i}^{(-1)}(t)\big]\cdot\mathbf{n}_{\neg i}^{(0)}(t), \\
\bar{\boldsymbol{\gamma}}_{\neg i} &:= \frac{L^3}{4}C_\perp\big\{\mathbf{n}_{\neg i}^{(-1)}(t)^{\mathrm{T}}\cdot\big[\mathbf{n}_i^{(0)}(t) + \mathbf{n}_i^{(-1)}(t)\big], -\mathbf{n}_{\neg i}^{(1)}(t)^{\mathrm{T}}\cdot\big[\mathbf{n}_i^{(0)}(t) + \mathbf{n}_i^{(1)}(t)\big]\big\}.
\end{aligned} \tag{A6}$$

APPENDIX B: INVERTIBILITY

In order to express the equations of motion in normal form, it is essential to establish the invertibility of the matrix $\mathcal{R}(t,\lambda)$, which can be written as

$$\mathcal{R}(t,\lambda) = \begin{bmatrix} \mathcal{R}_{11}(t) & -\lambda\mathcal{R}_{12}(t) \\ -\lambda\mathcal{R}_{21}(t) & \mathcal{R}_{22}(t) \end{bmatrix}. \tag{B1}$$

The matrices $\mathcal{R}_{ii}(t)$ for $i = 1, 2$, often referred to as grand resistance matrices [36] and encapsulating the overall resistance of the individual microswimmers, are independent of λ. Their positive definiteness and symmetry enable their inversion, thereby paving the way for establishing the invertibility of the entire matrix $\mathcal{R}(t,\lambda)$, as stated by the following theorem.

Theorem 1. There exists $0 < \lambda_0 < 1$ such that the matrix $\mathcal{R}(t,\lambda)$ is invertible for every $\lambda \in [0, \lambda_0)$ and for every $t \in [0, +\infty)$.

Proof. For $\lambda = 0$ the matrix $\mathcal{R}(t, 0)$ is diagonal and invertible; indeed its determinant is the product of the determinants $\det\mathcal{R}_{11}(t)\det\mathcal{R}_{22}(t)$, which is different from zero since the two block matrices are invertible. Thus there exists a λ_0 belonging

to the open interval (0,1) such that, for all λ within the interval $[0, \lambda_0)$ and every t in the interval $[0, +\infty)$, the determinant of the matrix $\mathcal{R}(t, \lambda)$ remains different from zero, concluding the proof.

As a consequence for $\lambda \in [0, \lambda_0)$, it results that

$$\begin{bmatrix} \dot{\mathbf{x}}_1(t) \\ \vartheta_1(t) \\ \dot{\mathbf{x}}_2(t) \\ \vartheta_2(t) \end{bmatrix} = -\mathcal{R}(t, \lambda)^{-1} \boldsymbol{\varphi}(t) \begin{bmatrix} \dot{\boldsymbol{\sigma}}_1(t) \\ \dot{\boldsymbol{\sigma}}_2(t) \end{bmatrix}. \tag{B2}$$

APPENDIX C: LIE BRACKETS' EXPANSION

Geometric control theory utilizes the principles of differential geometry to investigate the control of dynamic systems. A key concept in geometric control theory is the Lie bracket—a tool for measuring the interaction between two vector fields. By performing a Taylor expansion for short time intervals of the Lie brackets, we can derive explicit expressions for the system's displacement that encapsulate its behavioral characteristics [30]. According to Remark 3, $\gamma_i \tau$ is $O(\varepsilon)$. Thus we perform a Taylor expansion of the displacement up to $O(\gamma_i^2 \tau^2)$ and then further expand the components of the Lie brackets up to $O(\varepsilon^2)$, achieving an overall approximation of $O(\varepsilon^4)$. To enhance clarity, we present the expansion in four distinct stages (corresponding to the case discussed in Sec. III A 2), each encompassing a subinterval of time, as sketched in Fig. 3, and consider $\gamma_i = \gamma$ for $i = 1, \ldots, 4$.

1. First step

Referring to the first inset in Fig. 3, we get

$$\mathcal{S}(\gamma\tau) = \mathcal{S}(0) + \gamma\tau\dot{\mathcal{S}}(0) + \frac{\gamma^2\tau^2}{2}\ddot{\mathcal{S}}(0). \tag{C1}$$

Since both lower links move simultaneously with constant angular velocity, $\dot{\mathcal{S}}(0) = \mathbf{v}_1[\boldsymbol{\sigma}_1(0), \boldsymbol{\sigma}_2(0), \lambda] + \mathbf{v}_3[\boldsymbol{\sigma}_1(0), \boldsymbol{\sigma}_2(0), \lambda]$, Eq. (C1) becomes

$$\begin{aligned} \mathcal{S}(\gamma\tau) = \mathcal{S}(0) + \gamma\tau(\mathbf{v}_1[\boldsymbol{\sigma}_1(0), \boldsymbol{\sigma}_2(0), \lambda] + \mathbf{v}_3[\boldsymbol{\sigma}_1(0), \boldsymbol{\sigma}_2(0), \lambda]) + \frac{\gamma^2\tau^2}{2}(\nabla\mathbf{v}_1[\boldsymbol{\sigma}_1(0), \boldsymbol{\sigma}_2(0), \lambda](\mathbf{v}_1[\boldsymbol{\sigma}_1(0), \boldsymbol{\sigma}_2(0), \lambda] \\ + \mathbf{v}_3[\boldsymbol{\sigma}_1(0), \boldsymbol{\sigma}_2(0), \lambda]) + \nabla\mathbf{v}_3[\boldsymbol{\sigma}_1(0), \boldsymbol{\sigma}_2(0), \lambda](\mathbf{v}_1[\boldsymbol{\sigma}_1(0), \boldsymbol{\sigma}_2(0), \lambda] + \mathbf{v}_3[\boldsymbol{\sigma}_1(0), \boldsymbol{\sigma}_2(0), \lambda])), \end{aligned} \tag{C2}$$

where $\nabla\mathbf{v}_i$ denotes the gradient of the vector field $\mathbf{v}_i$.

2. Second step

Drawing upon the second inset in Fig. 3, we write

$$S(2\gamma\tau) = \mathcal{S}(\gamma\tau) + \gamma\tau\dot{\mathcal{S}}(\gamma\tau) + \frac{\gamma^2\tau^2}{2}\ddot{\mathcal{S}}(\gamma\tau). \tag{C3}$$

Since both upper links move simultaneously with constant angular velocity $\dot{\mathcal{S}}(\gamma\tau) = \mathbf{v}_2[\boldsymbol{\sigma}_1(\gamma\tau), \boldsymbol{\sigma}_2(\gamma\tau), \lambda] + \mathbf{v}_4[\boldsymbol{\sigma}_1(\gamma\tau), \boldsymbol{\sigma}_2(\gamma\tau), \lambda]$, Eq. (C3) becomes

$$\begin{aligned} \mathcal{S}(2\gamma\tau) = \mathcal{S}(\gamma\tau) + \gamma\tau(\mathbf{v}_2[\boldsymbol{\sigma}_1(\gamma\tau), \boldsymbol{\sigma}_2(\gamma\tau), \lambda] + \mathbf{v}_4[\boldsymbol{\sigma}_1(\gamma\tau), \boldsymbol{\sigma}_2(\gamma\tau), \lambda]) + \frac{\gamma^2\tau^2}{2}(\nabla\mathbf{v}_2[\boldsymbol{\sigma}_1(\gamma\tau), \boldsymbol{\sigma}_2(\gamma\tau), \lambda] \\ \times (\mathbf{v}_2[\boldsymbol{\sigma}_1(\gamma\tau), \boldsymbol{\sigma}_2(\gamma\tau), \lambda] + \mathbf{v}_4[\boldsymbol{\sigma}_1(\gamma\tau), \boldsymbol{\sigma}_2(\gamma\tau), \lambda]) + \nabla\mathbf{v}_4[\boldsymbol{\sigma}_1(\gamma\tau), \boldsymbol{\sigma}_2(\gamma\tau), \lambda](\mathbf{v}_2[\boldsymbol{\sigma}_1(\gamma\tau), \boldsymbol{\sigma}_2(\gamma\tau), \lambda] \\ + \mathbf{v}_4[\boldsymbol{\sigma}_1(\gamma\tau), \boldsymbol{\sigma}_2(\gamma\tau), \lambda])). \end{aligned} \tag{C4}$$

In Eq. (C4), where $\mathcal{S}(3\gamma\tau)$ is defined in Eq. (C2), we further expand the gradients of vectorial fields $\mathbf{v}_i[\boldsymbol{\sigma}_1(3\gamma\tau), \boldsymbol{\sigma}_2(3\gamma\tau), \lambda]$ $(i = 2, 4)$ around $\gamma\tau = 0$, retaining only terms up to order $\gamma^3\tau^3$. Thus we get

$$\begin{aligned} \mathcal{S}(2\gamma\tau) = \mathcal{S}(0) + \gamma\tau(\mathbf{v}_1[\boldsymbol{\sigma}_1(0), \boldsymbol{\sigma}_2(0), \lambda] + \mathbf{v}_3[\boldsymbol{\sigma}_1(0), \boldsymbol{\sigma}_2(0), \lambda]) + \frac{\gamma^2\tau^2}{2}(\nabla\mathbf{v}_1[\boldsymbol{\sigma}_1(0), \boldsymbol{\sigma}_2(0), \lambda] \\ \times (\mathbf{v}_1[\boldsymbol{\sigma}_1(0), \boldsymbol{\sigma}_2(0), \lambda] + \mathbf{v}_3[\boldsymbol{\sigma}_1(0), \boldsymbol{\sigma}_2(0), \lambda]) + \nabla\mathbf{v}_3[\boldsymbol{\sigma}_1(0), \boldsymbol{\sigma}_2(0), \lambda](\mathbf{v}_1[\boldsymbol{\sigma}_1(0), \boldsymbol{\sigma}_2(0), \lambda] \\ + \mathbf{v}_3[\boldsymbol{\sigma}_1(0), \boldsymbol{\sigma}_2(0), \lambda]) + \gamma\tau\mathbf{v}_2[\boldsymbol{\sigma}_1(0), \boldsymbol{\sigma}_2(0), \lambda] + \gamma\tau\nabla\mathbf{v}_2[\boldsymbol{\sigma}_1(0), \boldsymbol{\sigma}_2(0), \lambda](\mathbf{v}_1[\boldsymbol{\sigma}_1(0), \boldsymbol{\sigma}_2(0), \lambda] \\ + \mathbf{v}_3[\boldsymbol{\sigma}_1(0), \boldsymbol{\sigma}_2(0), \lambda]) + \mathbf{v}_4[\boldsymbol{\sigma}_1(0), \boldsymbol{\sigma}_2(0), \lambda] + \gamma\tau\nabla\mathbf{v}_4[\boldsymbol{\sigma}_1(0), \boldsymbol{\sigma}_2(0), \lambda](\mathbf{v}_1[\boldsymbol{\sigma}_1(0), \boldsymbol{\sigma}_2(0), \lambda] \\ + \mathbf{v}_3[\boldsymbol{\sigma}_1(0), \boldsymbol{\sigma}_2(0), \lambda]) + \frac{\gamma^2\tau^2}{2}\nabla\mathbf{v}_2[\boldsymbol{\sigma}_1(0), \boldsymbol{\sigma}_2(0), \lambda](\mathbf{v}_2[\boldsymbol{\sigma}_1(0), \boldsymbol{\sigma}_2(0), \lambda] + \mathbf{v}_4[\boldsymbol{\sigma}_1(0), \boldsymbol{\sigma}_2(0), \lambda]) \\ + \nabla\mathbf{v}_4[\boldsymbol{\sigma}_1(0), \boldsymbol{\sigma}_2(0), \lambda](\mathbf{v}_2[\boldsymbol{\sigma}_1(0), \boldsymbol{\sigma}_2(0), \lambda] + \mathbf{v}_4[\boldsymbol{\sigma}_1(0), \boldsymbol{\sigma}_2(0), \lambda])). \end{aligned} \tag{C5}$$

3. Third step

According to the third inset in Fig. 3, we get

$$S(3\gamma\tau) = \mathcal{S}(2\gamma\tau) + \gamma\tau\dot{\mathcal{S}}(2\gamma\tau) + \frac{\gamma^2\tau^2}{2}\ddot{\mathcal{S}}(2\gamma\tau). \tag{C6}$$

Given that both lower links move synchronously with constant angular velocity, $\dot{\mathcal{S}}(2\gamma\tau) = -\mathbf{v}_1[\boldsymbol{\sigma}_1(2\gamma\tau), \boldsymbol{\sigma}_2(2\gamma\tau), \lambda] - \mathbf{v}_3[\boldsymbol{\sigma}_1(2\gamma\tau), \boldsymbol{\sigma}_2(2\gamma\tau), \lambda]$, Eq. (C6) becomes

$$\begin{aligned}\mathcal{S}(3\gamma\tau) = \mathcal{S}(2\gamma\tau) &+ \gamma\tau(-\mathbf{v}_1[\boldsymbol{\sigma}_1(2\gamma\tau), \boldsymbol{\sigma}_2(2\gamma\tau), \lambda] - \mathbf{v}_3[\boldsymbol{\sigma}_1(2\gamma\tau), \boldsymbol{\sigma}_2(2\gamma\tau), \lambda]) + \frac{\gamma^2\tau^2}{2}(-\nabla\mathbf{v}_1[\boldsymbol{\sigma}_1(2\gamma\tau), \boldsymbol{\sigma}_2(2\gamma\tau), \lambda]\\ &\times (-\mathbf{v}_1[\boldsymbol{\sigma}_1(2\gamma\tau), \boldsymbol{\sigma}_2(2\gamma\tau), \lambda] - \mathbf{v}_3[\boldsymbol{\sigma}_1(2\gamma\tau), \boldsymbol{\sigma}_2(2\gamma\tau), \lambda]) - \nabla\mathbf{v}_3[\boldsymbol{\sigma}_1(2\gamma\tau), \boldsymbol{\sigma}_2(2\gamma\tau), \lambda]\\ &\times (-\mathbf{v}_1[\boldsymbol{\sigma}_1(2\gamma\tau), \boldsymbol{\sigma}_2(2\gamma\tau), \lambda] - \mathbf{v}_3[\boldsymbol{\sigma}_1(2\gamma\tau), \boldsymbol{\sigma}_2(2\gamma\tau), \lambda])).\end{aligned} \tag{C7}$$

In Eq. (C7), where $\mathcal{S}(3\gamma\tau)$ is defined in Eq. (C4), we further expand the gradients of vectorial fields $\mathbf{v}_i[\boldsymbol{\sigma}_1(3\gamma\tau), \boldsymbol{\sigma}_2(3\gamma\tau), \lambda]$ $(i = 2, 4)$ around $\gamma\tau = 0$, retaining only terms up to order $\gamma^3\tau^3$. Thus we get

$$\begin{aligned}\mathcal{S}(3\gamma\tau) = \mathcal{S}(2\gamma\tau) &+ \gamma\tau\{-[\mathbf{v}_1[\boldsymbol{\sigma}_1(0), \boldsymbol{\sigma}_2(0), \lambda] + \gamma\tau\nabla\mathbf{v}_1[\boldsymbol{\sigma}_1(0), \boldsymbol{\sigma}_2(0), \lambda](\mathbf{v}_1[\boldsymbol{\sigma}_1(0), \boldsymbol{\sigma}_2(0), \lambda]\\ &+ \mathbf{v}_3[\boldsymbol{\sigma}_1(0), \boldsymbol{\sigma}_2(0), \lambda])] + \gamma\tau\nabla\mathbf{v}_1[\boldsymbol{\sigma}_1(0), \boldsymbol{\sigma}_2(0), \lambda](\mathbf{v}_2[\boldsymbol{\sigma}_1(0), \boldsymbol{\sigma}_2(0), \lambda] + \mathbf{v}_4[\boldsymbol{\sigma}_1(0), \boldsymbol{\sigma}_2(0), \lambda])\}\\ &- (\mathbf{v}_3[\boldsymbol{\sigma}_1(0), \boldsymbol{\sigma}_2(0), \lambda]) + \gamma\tau\nabla\mathbf{v}_3[\boldsymbol{\sigma}_1(0), \boldsymbol{\sigma}_2(0), \lambda](\mathbf{v}_1[\boldsymbol{\sigma}_1(0), \boldsymbol{\sigma}_2(0), \lambda] + \mathbf{v}_3[\boldsymbol{\sigma}_1(0), \boldsymbol{\sigma}_2(0), \lambda])\\ &+ \gamma\tau\nabla\mathbf{v}_3[\boldsymbol{\sigma}_1(0), \boldsymbol{\sigma}_2(0), \lambda](\mathbf{v}_2[\boldsymbol{\sigma}_1(0), \boldsymbol{\sigma}_2(0), \lambda] + \mathbf{v}_4[\boldsymbol{\sigma}_1(0), \boldsymbol{\sigma}_2(0), \lambda])\\ &+ \frac{\gamma^2\tau^2}{2}[-\nabla\mathbf{v}_1[\boldsymbol{\sigma}_1(0), \boldsymbol{\sigma}_2(0), \lambda](-\mathbf{v}_1[\boldsymbol{\sigma}_1(0), \boldsymbol{\sigma}_2(0), \lambda] - \mathbf{v}_3[\boldsymbol{\sigma}_1(0), \boldsymbol{\sigma}_2(0), \lambda])]\\ &- \nabla\mathbf{v}_3[\boldsymbol{\sigma}_1(0), \boldsymbol{\sigma}_2(0), \lambda](-\mathbf{v}_1[\boldsymbol{\sigma}_1(0), \boldsymbol{\sigma}_2(0), \lambda] - \mathbf{v}_3[\boldsymbol{\sigma}_1(0), \boldsymbol{\sigma}_2(0), \lambda]).\end{aligned} \tag{C8}$$

4. Fourth step

Finally, in light of the fourth inset of Fig. 3, we can deduce

$$S(4\gamma\tau) = \mathcal{S}(3\gamma\tau) + \gamma\tau\dot{\mathcal{S}}(3\gamma\tau) + \frac{\gamma^2\tau^2}{2}\ddot{\mathcal{S}}(3\gamma\tau). \tag{C9}$$

Considering that both upper links move simultaneously with constant angular velocity, $\dot{\mathcal{S}}(3\gamma\tau) = -\mathbf{v}_2[\boldsymbol{\sigma}_1(3\gamma\tau), \boldsymbol{\sigma}_2(3\gamma\tau), \lambda] - \mathbf{v}_4[\boldsymbol{\sigma}_1(3\gamma\tau), \boldsymbol{\sigma}_2(3\gamma\tau), \lambda]$, Eq. (C9) becomes

$$\begin{aligned}\mathcal{S}(4\gamma\tau) = \mathcal{S}(3\gamma\tau) &+ \gamma\tau(-\mathbf{v}_2[\boldsymbol{\sigma}_1(3\gamma\tau), \boldsymbol{\sigma}_2(3\gamma\tau), \lambda] - \mathbf{v}_4[\boldsymbol{\sigma}_1(3\gamma\tau), \boldsymbol{\sigma}_2(3\gamma\tau), \lambda]) + \frac{\gamma^2\tau^2}{2}(-\nabla\mathbf{v}_2[\boldsymbol{\sigma}_1(3\gamma\tau), \boldsymbol{\sigma}_2(3\gamma\tau), \lambda]\\ &\times (-\mathbf{v}_2[\boldsymbol{\sigma}_1(3\gamma\tau), \boldsymbol{\sigma}_2(3\gamma\tau), \lambda] - \mathbf{v}_4[\boldsymbol{\sigma}_1(3\gamma\tau), \boldsymbol{\sigma}_2(3\gamma\tau), \lambda]) - \nabla\mathbf{v}_4[\boldsymbol{\sigma}_1(3\gamma\tau), \boldsymbol{\sigma}_2(3\gamma\tau), \lambda]\\ &\times (-\mathbf{v}_2[\boldsymbol{\sigma}_1(3\gamma\tau), \boldsymbol{\sigma}_2(3\gamma\tau), \lambda] - \mathbf{v}_4[\boldsymbol{\sigma}_1(3\gamma\tau), \boldsymbol{\sigma}_2(3\gamma\tau), \lambda])).\end{aligned} \tag{C10}$$

In Eq. (C10), where $\mathcal{S}(3\gamma\tau)$ is defined in Eq. (C8), we further expand the gradients of vectorial fields $\mathbf{v}_i[\boldsymbol{\sigma}_1(3\gamma\tau), \boldsymbol{\sigma}_2(3\gamma\tau), \lambda]$ $(i = 2, 4)$ around $\gamma\tau = 0$, retaining only terms up to order $\gamma^3\tau^3$. Thus we get

$$\begin{aligned}\mathcal{S}(4\gamma\tau) = \mathcal{S}(3\gamma\tau) &+ \gamma\tau\{-[\mathbf{v}_2[\boldsymbol{\sigma}_1(0), \boldsymbol{\sigma}_2(0), \lambda] + \gamma\tau\nabla\mathbf{v}_2[\boldsymbol{\sigma}_1(0), \boldsymbol{\sigma}_2(0), \lambda](\mathbf{v}_1[\boldsymbol{\sigma}_1(0), \boldsymbol{\sigma}_2(0), \lambda]\\ &+ \mathbf{v}_3[\boldsymbol{\sigma}_1(0), \boldsymbol{\sigma}_2(0), \lambda]) + \gamma\tau\nabla\mathbf{v}_2[\boldsymbol{\sigma}_1(0), \boldsymbol{\sigma}_2(0), \lambda](\mathbf{v}_2[\boldsymbol{\sigma}_1(0), \boldsymbol{\sigma}_2(0), \lambda] + \mathbf{v}_4[\boldsymbol{\sigma}_1(0), \boldsymbol{\sigma}_2(0), \lambda])\\ &+ \gamma\tau\nabla\mathbf{v}_2[\boldsymbol{\sigma}_1(0), \boldsymbol{\sigma}_2(0), \lambda](-\mathbf{v}_1[\boldsymbol{\sigma}_1(0), \boldsymbol{\sigma}_2(0), \lambda] - \mathbf{v}_3[\boldsymbol{\sigma}_1(0), \boldsymbol{\sigma}_2(0), \lambda])]\} - [\mathbf{v}_4[\boldsymbol{\sigma}_1(0), \boldsymbol{\sigma}_2(0), \lambda]\\ &+ \gamma\tau\nabla\mathbf{v}_4[\boldsymbol{\sigma}_1(0), \boldsymbol{\sigma}_2(0), \lambda](\mathbf{v}_1[\boldsymbol{\sigma}_1(0), \boldsymbol{\sigma}_2(0), \lambda] + \mathbf{v}_3[\boldsymbol{\sigma}_1(0), \boldsymbol{\sigma}_2(0), \lambda]) + \gamma\tau\nabla\mathbf{v}_4[\boldsymbol{\sigma}_1(0), \boldsymbol{\sigma}_2(0), \lambda]\\ &\times (\mathbf{v}_2[\boldsymbol{\sigma}_1(0), \boldsymbol{\sigma}_2(0), \lambda] + \mathbf{v}_4[\boldsymbol{\sigma}_1(0), \boldsymbol{\sigma}_2(0), \lambda]) + \gamma\tau\nabla\mathbf{v}_4[\boldsymbol{\sigma}_1(0), \boldsymbol{\sigma}_2(0), \lambda](-\mathbf{v}_1[\boldsymbol{\sigma}_1(0), \boldsymbol{\sigma}_2(0), \lambda]\\ &- \mathbf{v}_3[\boldsymbol{\sigma}_1(0), \boldsymbol{\sigma}_2(0), \lambda])] + \frac{\gamma^2\tau^2}{2}[-\nabla\mathbf{v}_2[\boldsymbol{\sigma}_1(0), \boldsymbol{\sigma}_2(0), \lambda](-\mathbf{v}_2[\boldsymbol{\sigma}_1(0), \boldsymbol{\sigma}_2(0), \lambda]\\ &- \mathbf{v}_4[\boldsymbol{\sigma}_1(0), \boldsymbol{\sigma}_2(0), \lambda]) - \nabla\mathbf{v}_4[\boldsymbol{\sigma}_1(0), \boldsymbol{\sigma}_2(0), \lambda](-\mathbf{v}_2[\boldsymbol{\sigma}_1(0), \boldsymbol{\sigma}_2(0), \lambda]\\ &- \mathbf{v}_4[\boldsymbol{\sigma}_1(0), \boldsymbol{\sigma}_2(0), \lambda])].\end{aligned} \tag{C11}$$

Finally, by replacing Eq. (C8) with $\mathcal{S}(3\gamma\tau)$ in the previous equation, we obtain the following expression:

$$\begin{aligned}\mathcal{S}(4\gamma\tau) = \mathcal{S}(0) &+ \gamma\tau^2(-\mathbf{v}_2[\boldsymbol{\sigma}_1(0), \boldsymbol{\sigma}_2(0), \lambda]\nabla\mathbf{v}_1[\boldsymbol{\sigma}_1(0), \boldsymbol{\sigma}_2(0), \lambda] + \mathbf{v}_1[\boldsymbol{\sigma}_1(0), \boldsymbol{\sigma}_2(0), \lambda]\\ &\times \nabla\mathbf{v}_2[\boldsymbol{\sigma}_1(0), \boldsymbol{\sigma}_2(0), \lambda] + \mathbf{v}_3[\boldsymbol{\sigma}_1(0), \boldsymbol{\sigma}_2(0), \lambda]\nabla\mathbf{v}_2[\boldsymbol{\sigma}_1(0), \boldsymbol{\sigma}_2(0), \lambda]\\ &- \mathbf{v}_2[\boldsymbol{\sigma}_1(0), \boldsymbol{\sigma}_2(0), \lambda]\nabla\mathbf{v}_3[\boldsymbol{\sigma}_1(0), \boldsymbol{\sigma}_2(0), \lambda] - \mathbf{v}_4[\boldsymbol{\sigma}_1(0), \boldsymbol{\sigma}_2(0), \lambda]\nabla\mathbf{v}_1[\boldsymbol{\sigma}_1(0), \boldsymbol{\sigma}_2(0), \lambda]\end{aligned}$$

$$+ \mathbf{v}_1[\boldsymbol{\sigma}_1(0), \boldsymbol{\sigma}_2(0), \lambda]\nabla\mathbf{v}_4[\boldsymbol{\sigma}_1(0), \boldsymbol{\sigma}_2(0), \lambda] - \mathbf{v}_4[\boldsymbol{\sigma}_1(0), \boldsymbol{\sigma}_2(0), \lambda] \times \nabla\mathbf{v}_3[\boldsymbol{\sigma}_1(0), \boldsymbol{\sigma}_2(0), \lambda] + \mathbf{v}_3[\boldsymbol{\sigma}_1(0), \boldsymbol{\sigma}_2(0), \lambda]\nabla\mathbf{v}_4[\boldsymbol{\sigma}_1(0), \boldsymbol{\sigma}_2(0), \lambda]), \tag{C12}$$

and so, while omitting explicit variable dependencies,

$$\mathcal{S}(4\gamma\tau) = \mathcal{S}(0) + \gamma^2\tau^2([\mathbf{v}_1(\cdot,\lambda), \mathbf{v}_2(\cdot,\lambda)] - [\mathbf{v}_2(\cdot,\lambda), \mathbf{v}_3(\cdot,\lambda)] + [\mathbf{v}_1(\cdot,\lambda), \mathbf{v}_4(\cdot,\lambda)] + [\mathbf{v}_3(\cdot,\lambda), \mathbf{v}_4(\cdot,\lambda)]). \tag{C13}$$

APPENDIX D: LIE BRACKETS' RELATIONSHIP

The derivation of Eq. (26) from Eq. (25) is presented here. Specifically, we elucidate the relationship between the Lie brackets in Eq. (25) and the Lie bracket in Eq. (26).

It is noteworthy that, when $\gamma_1 = \gamma_3$ and $\gamma_2 = \gamma_4$, we find

$$\gamma_1\gamma_2[\mathbf{v}_1(\cdot,\lambda), \mathbf{v}_2(\cdot,\lambda)] - \gamma_2\gamma_3[\mathbf{v}_2(\cdot,\lambda), \mathbf{v}_3(\cdot,\lambda)] + \gamma_1\gamma_4[\mathbf{v}_1(\cdot,\lambda), \mathbf{v}_4(\cdot,\lambda)] + \gamma_3\gamma_4[\mathbf{v}_3(\cdot,\lambda), \mathbf{v}_4(\cdot,\lambda)] = \gamma_1\gamma_2([\mathbf{v}_1(\cdot,\lambda), \mathbf{v}_2(\cdot,\lambda)] - [\mathbf{v}_2(\cdot,\lambda), \mathbf{v}_3(\cdot,\lambda)] + [\mathbf{v}_1(\cdot,\lambda), \mathbf{v}_4(\cdot,\lambda)] + [\mathbf{v}_3(\cdot,\lambda), \mathbf{v}_4(\cdot,\lambda)]). \tag{D1}$$

Through explicit calculations, while omitting the dependence on other variables of the vector fields $\mathbf{v}_i$, we arrive at the identity

$$\nabla\mathbf{v}_2\mathbf{v}_1 - \nabla\mathbf{v}_1\mathbf{v}_2 - \nabla\mathbf{v}_3\mathbf{v}_2 + \nabla\mathbf{v}_2\mathbf{v}_3 + \nabla\mathbf{v}_4\mathbf{v}_1 - \nabla\mathbf{v}_1\mathbf{v}_4 + \nabla\mathbf{v}_4\mathbf{v}_3 - \nabla\mathbf{v}_3\mathbf{v}_4 = \nabla\mathbf{v}_2(\mathbf{v}_1 + \mathbf{v}_3) - \nabla\mathbf{v}_1(\mathbf{v}_2 + \mathbf{v}_4) - \nabla\mathbf{v}_3(\mathbf{v}_2 + \mathbf{v}_4) + \nabla\mathbf{v}_4(\mathbf{v}_1 + \mathbf{v}_3), \tag{D2}$$

where $\nabla\mathbf{v}_i$ denotes the gradient of the vector field $\mathbf{v}_i$. It is straightforward to observe that, upon substituting $\mathbf{s}_1 := \mathbf{v}_1 + \mathbf{v}_3$ and $\mathbf{s}_2 := \mathbf{v}_2 + \mathbf{v}_4$, Eq. (D2) reduces to

$$\mathbf{s}_1(\nabla\mathbf{v}_2 + \nabla\mathbf{v}_4) - \mathbf{s}_2(\nabla\mathbf{v}_1 + \nabla\mathbf{v}_3) = \mathbf{s}_1\nabla\mathbf{f}_2 - \mathbf{s}_2\nabla\mathbf{f}_1 = [\mathbf{s}_1, \mathbf{s}_2]. \tag{D3}$$

[1] D. Tam and A. E. Hosoi, Phys. Rev. Lett. **98**, 068105 (2007).
[2] C. Moreau, J. Phys. Soc. Jpn. **92**, 121005 (2023).
[3] B. Qian, H. Jiang, D. A. Gagnon, K. S. Breuer, and T. R. Powers, Phys. Rev. E **80**, 061919 (2009).
[4] R. Golestanian, J. M. Yeomans, and N. Uchida, Soft Matter **7**, 3074 (2011).
[5] B. M. Friedrich and F. Jülicher, Phys. Rev. Lett. **109**, 138102 (2012).
[6] R. Wichterman, *The Biology of Paramecium* (Plenum Press, New York, 1986).
[7] H. Riedel, K. Kruse, and J. Howard, Science **309**, 300 (2005).
[8] A. J. T. M. Mathijssen, A. Doostmohammadi, J. M. Yeomans, and T. N. Shendruk, J. Fluid Mech. **806**, 35 (2016).
[9] A. Daddi-Moussa-Ider, H. Löwen, and B. Liebchen, Commun. Phys. **4**, 15 (2021).
[10] F. Qiu, R. Mhanna, L. Zhang, Y. Ding, S. Fujita, and B. J. Nelson, Sens. Actuators, B **196**, 676 (2014).
[11] C. Dillinger, N. Nama, and D. Ahmed, Nat. Commun. **12**, 6455 (2021).
[12] F. Alouges, A. DeSimone, L. Giraldi, and M. Zoppello, Soft Robotics **2**, 117 (2015).
[13] J. Grover, J. Zimmer, T. Dear, M. Travers, H. Choset, and S. D. Kelly, *2018 Annual American Control Conference (ACC)* (IEEE, New York, 2018), pp. 6067–6074.
[14] F. Alouges, A. DeSimone, L. Giraldi, and M. Zoppello, *2017 Proceedings of the IFAC 20th World Congress* (Elsevier, Amsterdam, 2017), pp. 4120–4125.
[15] R. Maggistro and M. Zoppello, IEEE Control Syst. Lett. **3**, 841 (2019).
[16] L. Giraldi, P. Martinon, and M. Zoppello, *52nd IEEE Conference on Decision and Control* (IEEE, New York, 2013), pp. 3870–3875.
[17] I. S. Khalil, A. Fatih Tabak, A. Klingner, and M. Sitti, Appl. Phys. Lett. **109**, 033701 (2016).
[18] A. Das, M. Styslinger, D. M. Harris, and R. Zenit, Rev. Sci. Instrum. **93**, 044103 (2022).
[19] S. Lim, A. Yadunandan, and M. K. Jawed, Soft Matter **19**, 2254 (2023).
[20] U. K. Cheang and M. J. Kim, Appl. Phys. Lett. **109**, 034101 (2016).
[21] U. K. Cheang, D. Roy, J. H. Lee, and M. J. Kim, Appl. Phys. Lett. **97**, 213704 (2010).
[22] Y. Yang, V. Marceau, and G. Gompper, Phys. Rev. E **82**, 031904 (2010).
[23] M. Zoppello, M. Morandotti, and H. Bloomfield-Gadêlha, Meccanica **57**, 2187 (2022).
[24] E. M. Purcell, Am. J. Phys. **45**, 3 (1977).
[25] E. Lauga and R. E. Goldstein, Phys. Today **65**(5), 30 (2012).
[26] T. Niedermayer, B. Eckhardt, and P. Lenz, Chaos **18**, 037128 (2008).
[27] J. Gray and G. J. Hancock, J. Exp. Biol. **32**, 802 (1955).
[28] F. Alouges, A. DeSimone, L. Giraldi, and M. Zoppello, Int. J. Non Linear Mech. **56**, 132 (2013).
[29] Y. Man, L. Koens, and E. Lauga, EPL (Europhys. Lett.) **116**, 24002 (2016).
[30] J.-M. Coron, *Control and Nonlinearity* (American Mathematical Society, Providence, RI, 2007), p. 136.

[31] L. Giraldi, P. Martinon, and M. Zoppello, Phys. Rev. E **91**, 023012 (2015).
[32] W. Magnus, Commun. Pure Appl. Math. **7**, 649 (1954).
[33] R. Mason and J. Burdick, *Proceedings of the 1999 IEEE International Conference on Robotics and Automation* (IEEE, New York, 1999).
[34] O. Wiezel, S. Ramasamy, N. Justus, Y. Or, and R. L. Hatton, Automatica **158**, 111223 (2023).
[35] G. I. Taylor, Proc. R. Soc. London Ser. A **209**, 447 (1951).
[36] J. Happel and H. Brenner, *Low Reynolds Number Hydrodynamics: With Special Applications to Particulate Media* (Springer Science & Business Media, New York, 1983), Vol. 1.